Materials Horizons

ROYAL SOCIETY OF CHEMISTRY

REVIEW

View Article Online
View Journal

Cite this: DOI: 10.1039/d4mh00916a

Nanoionics enabled atomic point contact construction and quantum conductance effects

Runsheng Gao,†[ab] Xiaoyu Ye,†[ab] Cong Hu,†[ab] Ziyi Zhang,[abc] Xinhui Ji,[abc] Yanyu Zhang,[abc] Xiaohan Meng,[abd] Huali Yang,[abc] Xiaojian Zhu *[abc] and Run-Wei Li *[abc]

Received 16th July 2024,
Accepted 16th September 2024

DOI: 10.1039/d4mh00916a

rsc.li/materials-horizons

The miniaturization of electronic devices is important for the development of high-density and function-integrated information devices. Atomic-point-contact (APC) structures refer to narrow contact areas formed by one or more atoms between two conductive electrodes that produce quantum conductance effects when the electrons pass through the APC channel, providing a new development path for the miniaturization of information devices. Recently, nanoionics has enabled the electric field reconfiguration of APC structures in solid-state electrolytes, offering new approaches to controlling the quantum conductance states, which may lead to the development of emerging information technologies with low power consumption, high speed, and high density. This review provides an overview of APC structures with a focus on the fabrication methods enabled by nanoionics technology. In particular, the advantages of electric field-driven nanoionics in the construction of APC structures are summarized, and the influence of external fields on quantum conductance effects is discussed. Recent studies on electric field regulation of APC structures to achieve precise control of quantum conductance states are also reviewed. The potential applications of quantum conductance effects in memory, computing, and encryption-related information technologies are further explored. Finally, the challenges and future prospects of quantum conductance effects in APC structures are discussed.

Wider impact

Atomic point contacts (APCs) represent pivotal structures at the atomic scale, allowing electrons to pass through the quantized energy levels and producing quantum conductance effects. Unlike traditional approaches, nanoionics offers a simple and effective way to build APCs by driving ion migration using localized electric fields. To date, APCs have been successfully developed using various nanoionic materials and have been employed in creating innovative devices, such as resistive switching memories. The quantum conductance of APCs constructed *via* the nanoionics method features multi-level states and tunable properties, which contribute to developing novel devices with high scalability, fast switching speeds, and low energy consumption.

This review provides a comprehensive summary of the advancements in quantum conductance effects within APCs fabricated through the nanoionics technique. It covers the fundamental mechanisms of ion migration, explores the impact of various external fields on quantum effects in APCs, and highlights their significant applications across diverse research areas. Additionally, this review discusses current challenges and offers insights into future development trends. This review will enhance our understanding of quantum conductance effects in APCs and serve as a valuable reference for the design of miniaturized and multifunctional information devices.

1. Introduction

The rapid growth of artificial intelligence (AI), the Internet of Things (IoT), and autonomous vehicles (AV) has produced massive amounts of data that need to be processed. Over the past few decades, Moore's Law and Dennard's principles have led to the vigorous development of the semiconductor industry. They point out the enhancement of electron and hole mobility within channels and the utilization of high dielectric constant materials to minimize the thickness and size of the devices. Consequently, information devices have undergone continuous

[a] CAS Key Laboratory of Magnetic Materials and Devices, Ningbo Institute of Materials Technology and Engineering, Chinese Academy of Sciences, Ningbo 315201, China. E-mail: zhuxj@nimte.ac.cn, runweili@nimte.ac.cn
[b] Zhejiang Province Key Laboratory of Magnetic Materials and Application Technology, Ningbo Institute of Materials Technology and Engineering, Chinese Academy of Sciences, Ningbo 315201, China
[c] College of Materials Science and Opto-Electronic Technology, University of Chinese Academy of Sciences, Beijing 100049, China
[d] School of Physical Science and Technology, ShanghaiTech University, Shanghai 201210, China
† These authors contributed equally.

miniaturization, scaling down to nanometer sizes.[1] However,[2] the current technical trajectory of integrated circuit technology is facing significant challenges due to the inherent limitations in indefinitely shrinking the size of physical components.[3] Therefore, exploring new technological pathways is essential to advance the miniaturization of information devices and meet future needs such as high-density information storage and high-performance computing.

Atomically precise manufacturing, achieved through precise manipulation of atoms and nanostructures, is emerging as a significant approach for advancing manufacturing technologies.[4] At this scale, various quantum effects manifest, generating novel physical and chemical properties with potential applications.[5] Quantum mechanics determines the fundamental laws governing the behavior of matter and fields at the particle, atomic, and molecular scales. Using the unique quantum effects offers fundamental performance advantages over conventional classical machines.[6] In recent years, the fundamental properties of quantum effects, such as quantum coherence, quantum entanglement, and quantum statistics, have been harnessed to conduct plenty of cutting-edge research studies in fields like quantum computing, quantum communication, and quantum precision measurement.[7] For instance, a single-atom device with excellent quantum coherence has been constructed.[8] This would lead to the emergence of hundreds of high-quality quantum logic qubits within a highly coherent quantum volume, enabling quantum computers to leverage quantum advantages over traditional computers.[9] Meanwhile, the quantum conductance effect with many advantages could be produced when the electrons are limited to a narrow constriction, which has a width equal to the electrons' Fermi wavelength and a length much smaller than the mean free path. The conductance is quantized in units of G_0, where G_0 denotes the conductance quantum ($G_0 = 2e^2/h$, where e and h

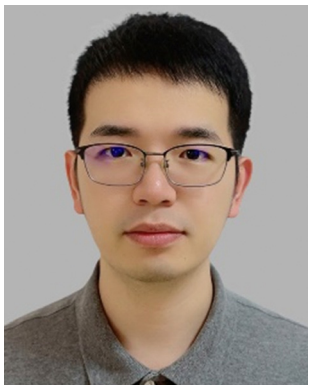

Runsheng Gao

Runsheng GAO is currently an Associate Professor at the Ningbo Institute of Materials Technology and Engineering, Chinese Academy of Sciences. He received his PhD degree from the University of Tsukuba in 2020, Japan. Then, he served as a postdoctoral researcher at the National Institute for Materials Science (NIMS) in Japan. His primary research interests revolve around investigating ion migration and storage mechanisms in diverse nanoionic materials, focusing on the fabrication of related devices and exploration of application scenarios.

Xiaoyu Ye

Xiaoyu Ye received her BS degree in material forming and control engineering from Shandong University, Jinan, China, in 2016, and her PhD degree in materials physics and chemistry from the University of Chinese Academy of Sciences, China, in 2023. Since then, she has been working in the Key Laboratory of Magnetic Materials and Devices, Chinese Academy of Sciences, China, as a postdoctoral researcher. Her current research interests are mainly in memristive materials and devices.

Cong Hu

Cong Hu is currently an Assistant Professor at the Ningbo Institute of Materials Technology and Engineering (NIMTE), Chinese Academy of Sciences (CAS). He graduated from the University of Chinese Academy of Sciences (UCAS) with a PhD degree in 2020, worked as a postdoctoral researcher at Westlake University from 2021 to 2023, and then joined the Laboratory of Magnetic Materials and Devices of NIMTE. His research mainly focuses on the theoretical simulation of electronic structure properties and phase transition by first-principles methods.

Xiaojian Zhu

Xiaojian Zhu received his BS degree in physics from Soochow University, China, in 2009, and his PhD degree in materials science from the University of Chinese Academy of Sciences, China, in 2014. From 2015 to 2020, he worked as a postdoctoral research fellow at the Electrical Engineering and Computer Science Department, University of Michigan. He is currently a Full Professor at the Ningbo Institute of Materials Technology and Engineering, Chinese Academy of Sciences. His research interests include nanoionic materials and devices for neuromorphic computing.

are the electron charge and Planck's constant, respectively). With the continuous advancements in research technology and exploration, quantum conductance phenomena have been observed in nanostructures, such as quantum point contact structures,[10,11] metal nanowires,[12,13] and graphene,[14] at room temperature or even higher. This is in contrast to with two-dimensional electron gas (2DEG) systems, which typically require extremely low temperatures. Experimental results also confirm the precise controllability and multi-level adjustability of quantum conductance states,[15] offering diverse options for applications in information storage, computing, and encryption.

Due to the atomic-point-contact (APC) structures operating at the scale of just one or a few atoms, scattering of electrons is minimized as they pass through the APC channel. They serve as an ideal platform for producing and studying quantum conductance effects. Traditionally, APC structures are fabricated using the mechanically controlled break junction (MCBJ) method, which forms the APC structures by separating and reconnecting metal components.[16,17] However, this method needs strict operating conditions that limit its practical application. Nanoionics is a research field that centers on the study and application of phenomena associated with the transport of ions in nanoscale materials, focusing on their movement, manipulation, and interactions within these materials. It has diverse applications, including energy storage and conversion systems, sensors, biomedical applications, and information storage systems.[18–21] Recent studies indicate that nanoionics-based memory devices, such as resistive switching devices, offer significant advantages including small size, high speed, and low-power operation.[22] These benefits help address the scaling limitations of conventional electronic information devices. Consequently, nanoionic devices have garnered renewed interest across various application areas. A key trend in this field is the development of precise ion manipulation techniques aimed at constructing advanced functional nanostructures and exploring new devices with enhanced performance.

Nanoionics technology has been employed since the 1970s to develop various devices, including electrochemical integral elements and memory storage systems.[23] Nanoionics-based APC structures are constructed through electric field-driven ion migration in solid-state electrolytes. The ions are propelled by the external electric field to migrate between the two electrodes, generating the conductive APC structures through redox reactions, which reduce the dominant electron transport scattering mode within the atomic-scale channel.[24–26] In 1998, Li *et al.* fabricated narrow metal-coated copper nanowires *via* electrochemical deposition of Cu ions, resulting in a narrower structure and the formation of an APC structure, which enabled the emergence of quantized conductance.[27] Then, many models were proposed to explain this phenomenon, such as conductive filament, charge trapping defect states, and charge trapping states at metal/oxide interfaces with a change in the Schottky-like barrier.[28,29] Terabe *et al.* developed a silver sulfide/silver/platinum (Ag_2S/Ag/Pt) atomic switch device by the scanning tunneling microscopy (STM) method in 2001,[30] and then presented a more easily integrated crossbar structure by solid-state electrochemical methods in 2005.[15] This device demonstrated highly controllable quantum conductance states compared to those achieved using other methods.[31,32] The sandwich structure allows switching operations and quantum conductance states to be controlled by applying voltage to the electrodes, facilitating the study of quantum conductance in APC structures. To date, various APC structures have been fabricated by driving different ions using electric fields.[33] These structures have confirmed that the nanoionics method could efficiently realize the quantum conductance effects associated with ballistic electron transport.[34] Compared to general techniques, the nanoionics migration offers precise modulation of the APC structures. Additionally, the electric field-driven approach allows for greater diversity in the composition, elements, and structure of APCs, enabling the development of various nanoionic devices for new applications (Fig. 1).[35,36] Nanoionics-based devices also exhibit high scalability, fast switching speeds, and low energy consumption.[37,38]

Herein, this review paper introduces the construction mechanisms and procedures of atomic-point-contact (APC) structures using the electric field-driven ion strategy. It discusses the development and applications of quantum conductance effects within these structures. The advantages of using electric field-driven ions for APC construction are analyzed and summarized. Particularly, the effects of various external physical fields on the optimization and regulation of APC construction and quantum conductance are further discussed. Finally, diverse applications and extensive development prospects for quantum conductance across various fields are also outlined. This review provides valuable insights for the future research,

Run-Wei Li

Run-Wei Li received his PhD degree from the Institute of Physics (IOP), CAS in 2002. Prof. Li served as a Japan Society for the Promotion of Science (JSPS) research fellow in Osaka University, Japan (2002–2003); a Humboldt Fellow in Kaiserslautern University, Germany (2003–2005); and a Senior Research Fellow in the International Center for Young Scientists, National Institute for Materials Sciences, Japan (2005–2008). In 2008, he joined the Ningbo Institute of Materials Technology and Engineering (NIMTE), CAS, as a full-time professor. Currently, he serves as a Member of the Asian Union of Magnetics Societies (AUMS) Council, the Senior Member of the Institute of Electrical and Electronics Engineers (IEEE), the Fellow of the Chinese Institute of Electronics (CIE), the Vice Chairman of the Applied Magnetics Committee of the CIE and the Magnetics Committee of the Chinese Physical Society (CPS), and the Editorial Board Member of Sensors and Journal of Semiconductors. His research focuses on flexible magnetic and electronic materials and devices for information storage and sensor technologies.

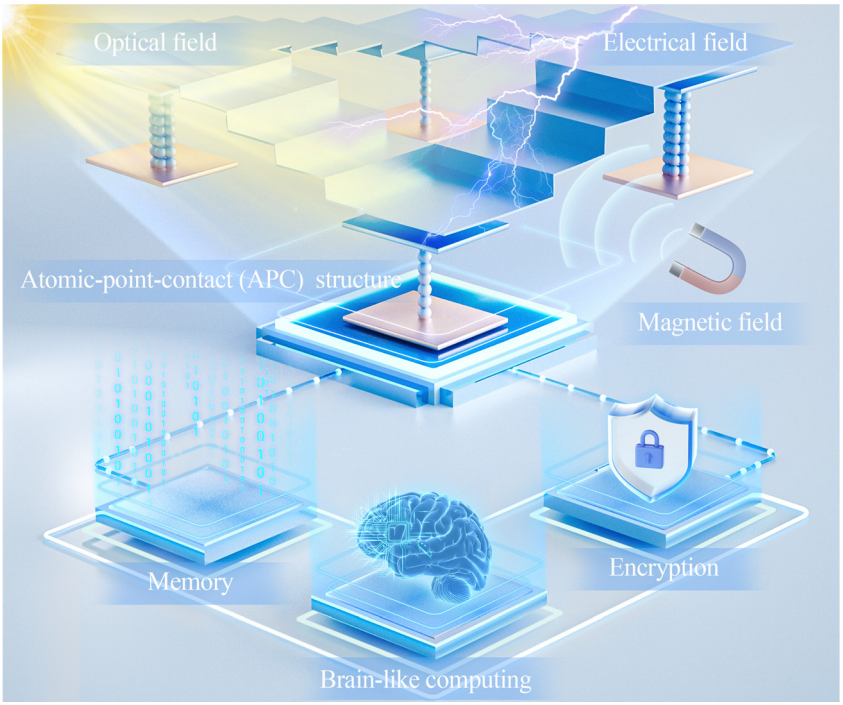

Fig. 1 Atomic point contact (APC) structures and the quantum conductance effects are influenced by a variety of physical fields, including optical, electric, and magnetic fields. These effects have been utilized in applications such as memory, computing, and encryption.

development, and applications of nanoionics-enabled quantum device manufacturing.

2. Traditional construction methods and theory of APC structures

The APC typically refers to a structure where two electrical contacts are connected by a 'neck' consisting of several atoms with a width equal to the electrons' Fermi wavelength. This configuration is often associated with various quantum effects, such as ballistic electron transport, quantum conductance, and thermal conductance quantization.[39] The first experimental measurements of the quantum conductance effect in narrow constrictions were conducted in a 2DEG within GaAs–AlGaAs heterostructures (Fig. 2a and b).[34,40] Besides this, the quantum conductance effect was also detected when the size of the nanowires was down to the APC structures. As shown in Fig. 2c, when the length of the APC is less than the electron mean free path and its lateral dimension is equal to the Fermi wavelength, the electrons can pass through the point contact by ballistic transportation without colliding and scattering, rather than by diffusive transport, which is typically on a larger scale. Ohnishi *et al.*[41] reported the quantum conductance effect in a metal APC structure, allowing the direct observation of the relationship between electron transport and contact structure. Fig. 2d shows a plot of the conductance change as the tip is withdrawn, indicating that the conductance of the point contact varies with its lateral size in integer multiples of G_0. The conductance of a single strand of atoms is 1 G_0, while a double strand exhibits twice this conductance. The models of the APC structure for single and double strands of gold atoms are shown in the inset images, corresponding to 1 and 2 G_0, respectively. Currently, it can be prepared by several traditional construction methods, such as MCBJ, STM, electrochemical deposition, and photolithography techniques.[42]

2.1. Mechanically controlled break junction technique

The mechanically controlled break-junction (MCBJ) technique has been widely used to construct metallic APC structures and produce the quantum conductance effect. In general, the metallic nanowire with a notch is mechanically broken into two pieces. The two pieces are then brought back into contact by utilizing piezoelectric elements that precisely control the distance. This process results in the formation of a metallic APC structure.[43,44] The MCBJ technique has facilitated the discovery of quantized conductance in various metallic wires, including sodium, gold, copper, lead, platinum, aluminium, and niobium (Na, Au, Cu, Pb, Pt, Al, and Nb).[45–47] For example, Muller *et al.* have successfully constructed the Au and Cu metallic APC structures through the MCBJ method. The quantum conductance effect was detected at room temperature, while the conductance of the contacts showed clear plateaus near the integer multiples of G_0.[48] Strigl *et al.* also conducted an investigation of the APC structure by stretching Pt nano-bridges fabricated by the MCBJ method (Fig. 3a). The pristine Pt nano-bridge exhibited a conductance of approximately 200 G_0 before rupture. The cross-section of the junction was

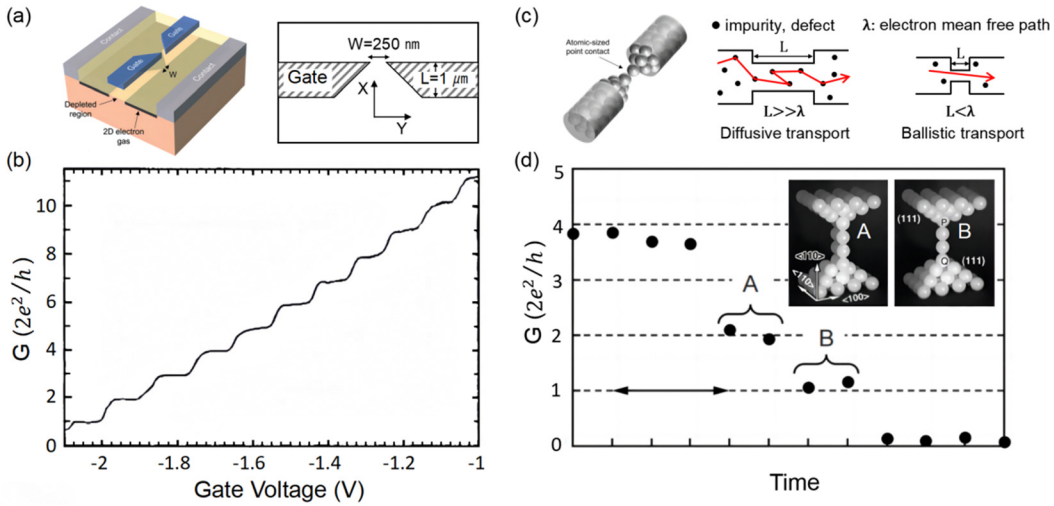

Fig. 2 Quantum conductance effect in the APC structures. (a) The illustration diagram of the heterostructure, where a 2DEG-based APC structure is formed at the interface of the heterostructure.[34] (b) The relationship between conductance and the gate voltage.[40] (c) The schematic diagram of the APC structures and ballistic electron transport.[34] (d) The relationship between conductance and the lateral size of the APC structures.[41]

carefully adjusted by stretching the Pt nano-bridge while simultaneously measuring its conductance. As the atomic contact was further elongated, a monoatomic Pt chain was formed once the conductance dropped below 2.5 G_0. Using this technique, Pt chains could be consistently created up to seven atoms in length.[49] Despite its advantages, precise control of the APC at the atomic scale remains challenging due to piezoelectric element fatigue. Additionally, the integration of the MCBJ method with conventional complementary metal–oxide semiconductor (CMOS) processes and other electronic devices to achieve functionalities such as information storage and computing remains a challenge. These limitations affect the practical applications of the MCBJ method.

2.2. Scanning tunneling microscopy method

Scanning tunneling microscopy (STM) is a widely used scanning probe microscopy technique that provides significantly enhanced resolution compared to other atomic force microscopy techniques. It allows the observation and manipulation of individual atoms with high precision, particularly at low temperatures. In 1990, Eigler *et al.* demonstrated the manipulation of individual xenon atoms on a single crystal nickel surface using the STM method at a low temperature of 4 K.[51] They successfully fabricated rudimentary structures atom by atom, confirming that the APC structure can also be constructed using the STM's atomic manipulation method. By applying a voltage pulse with suitable amplitude and duration between the STM tip and the sample, an electric field with a range from 10^9 to 10^{10} V m^{-1} can be generated. The strong electric field facilitates the extraction of adsorbed atoms from the sample surface, which are then displaced by the STM tip. Furthermore, Terabe *et al.* proposed an APC structure using nanoionics and solid electrochemical reactions with a STM in an Ag_2S/Ag/Pt device.[30] When a negative bias is applied to the Pt electrode, Ag ions in Ag_2S are reduced to Ag atoms by electrons from the Pt electrode, leading to the deposition of Ag atoms on the surface of Ag_2S. These Ag atoms form an atomic bridge that exhibits quantized conductance in units of G_0. Applying the reverse bias results in the ionization and dissolution of the Ag atoms in the bridge, causing it to become thinner and eventually break.

In addition, Waser *et al.* constructed a Ta APC structure between the STM tip and a 2 nm amorphous TaO_x film (Fig. 3b). Initially, a voltage of 1 V did not cause the rearrangement of atoms. Upon applying a voltage of −3 V, an instantaneous increase in the tunneling current was observed. Subsequently, the current decreased to 104 nA when a −1 mV read voltage was applied. Based on the aforementioned measurement results, the conductance value was calculated to be 1.3 G_0. This value exceeds that of a single APC, indicating that both Ta ion migration and electrochemical processes occurred within the TaO_x film, forming a Ta metallic APC structure. Ta-based APC structures typically display poor stability due to a high propensity for spontaneous reduction. As a result, the point contact was rendered inoperable after a period of one second.[11] Tang *et al.* employed a combination of electron beam thinning techniques with STM to fabricate the APC structures.[50] Carbon nanotubes (CNTs) acted as both nano-connectors and electrodes, forming a CNT-clamped metal atomic chain, including Fe, Co, Ni, and their alloys. The metal nanorods were initially filled into the CNTs, and the surrounding carbon shell was subsequently removed to expose the metal nanorods and make them thin using strong electron irradiation within a transmission electron microscope (TEM). Finally, they successfully fabricated a CNT-clamped metal atomic chain. During the thinning process, the formation of APC structures and quantum conductance effects were observed, as depicted in Fig. 3c. However, STM methods also have several challenges, such as stability which is susceptible to destruction from environmental disturbances. Advanced automation technologies are needed to prepare large-scale and intricate structures with atomic-level precision.

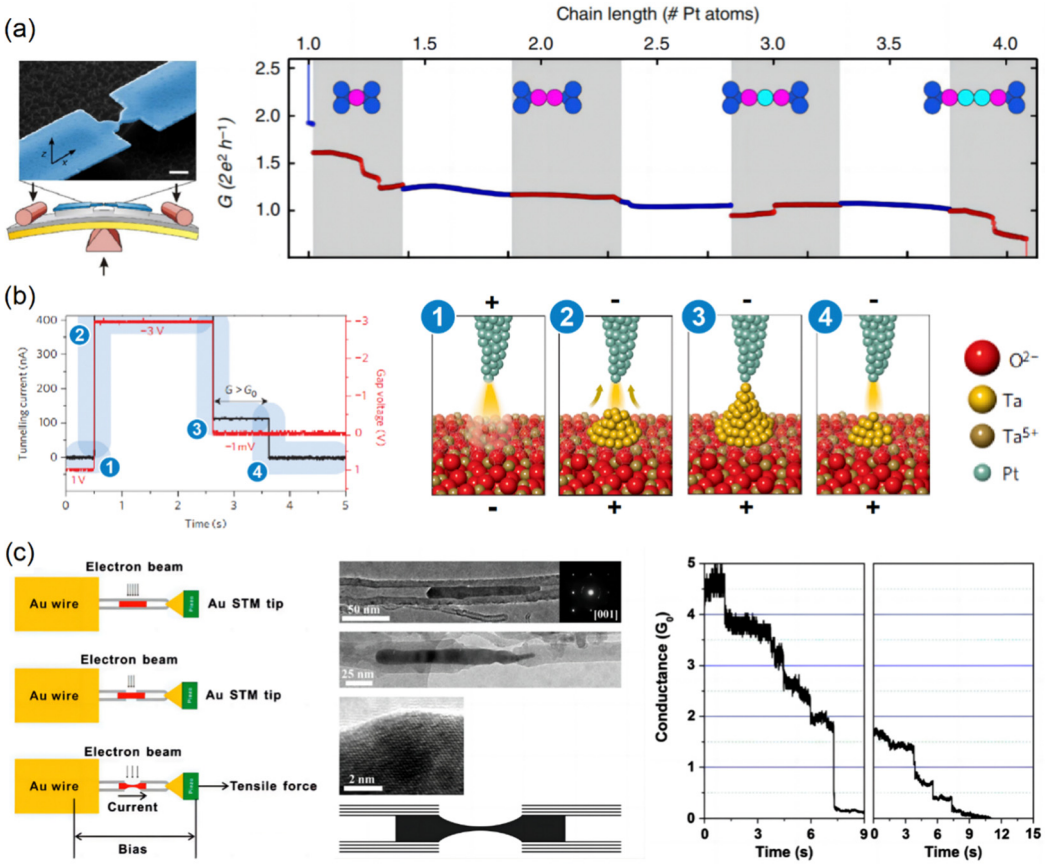

Fig. 3 Traditional methods for constructing APC structures. (a) Formation of mono-atomic chains and observation of quantum conductance effects *via* the MCBJ technique. The schematic shows the experimental setup and an electron micrograph of a suspended Pt nano-bridge (left). The conductance varies with the chain length (right).[49] (b) Construction method of APC structures using STM. A Ta metallic APC structure was formed between the STM tip and a 2 nm TaO_x layer due to Ta ion diffusion and chemical reactions.[11] (c) Schematic diagram of the APC structures constructed through electron irradiation and STM methods (left). The fabrication process of a CNT-clamped Fe nanorod (middle). The conductance changes as a function of time during the formation and thinning of atomic chains at a constant bias of 12 mV (right).[50]

Except for the MCBJ and STM methods, APC structures can also be constructed by electrochemical deposition in a liquid electrolyte. By immersing electrode pairs at a distance of hundreds of nanometers in a metal salt solution, the deposition of metals on the electrode surfaces is achieved by electrochemical reactions under the electric field. When these deposited metals come into contact, an APC structure is formed.[52,53] Nevertheless, this approach is predominantly applicable in liquid environments and presents compatibility challenges with CMOS technologies.

2.3. Theoretical mechanism

The Landauer–Büttiker (LB) method is a theoretical framework used to describe electron transport in mesoscopic systems that is suitable for quantum conductance effects.[54] The LB method extends the original Landauer formula, which relates the conductance of a conductor to the transmission probabilities of electrons through it. As shown in Fig. 4a, the left and right electrodes are ideal electron reservoirs that can absorb electrons flowing into them. Two ideal conductors (quantum leads) are connected to the middle elastic scatterer and electron reservoir. Electrons are emitted from one electrode, pass through an ideal conductor without scattering, and are partially reflected by the scattering centers with a reflection rate of R and a transmission rate of T (Fig. 4b), and the transmitted electrons enter the other electrode and are completely absorbed. Assuming that the chemical potentials of the two electron reservoirs are μ_1 and μ_2, an external voltage is applied such that $\mu_1 - \mu_2 =$ eV. When the quantum lead is a one-dimensional ideal conductor, due to the quantum size effect perpendicular to the transport direction, electrons in the one-dimensional ideal conductor exhibit discrete energy levels E_n, and the full energy is given by

$$E_n(k) = E_n + \frac{\hbar^2 k^2}{2m^*} = E_n + \varepsilon_k$$

where E_n is the transverse energy eigenvalue, ε_k is the kinetic energy for longitudinal motion, $\hbar = h/(2\pi)$, h is Planck's constant, and k and m^* are the electron wavevector and effective mass, respectively.

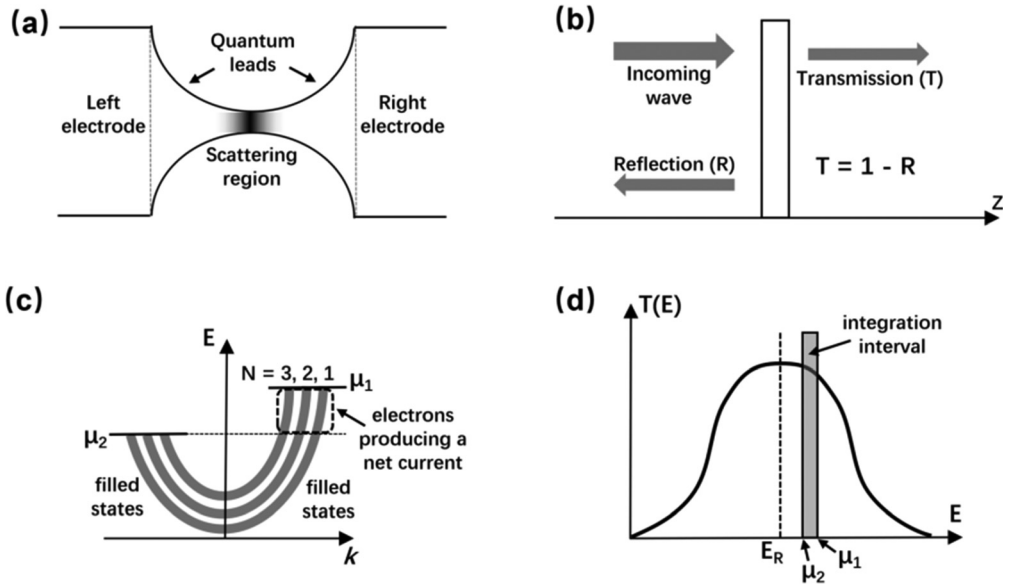

Fig. 4 Model of the quantum transport in a nanodevice.[54,55] (a) Schematic picture of an APC. The scattering region is connected to the electrodes through the quantum leads; (b) reflection and transmission amplitudes; (c) energy band diagram of a ballistic device with a finite number of populated 1D sub-bands; (d) energy interval over which the transmission must be integrated to obtain the overall current.

The one-dimensional sub-band between μ_1 and μ_2 can be used as a channel for propagating electrons (Fig. 4c),[55] in which case the intermediate scatterer can be seen as a potential barrier. If the two lowest discrete energy levels are spaced E_2–E_1 sufficiently large such that all electrons fall within the one-dimensional sub-band of E_1, this is an example of one conducting channel (Fig. 4d). The net current can be expressed as

$$I = 2eT\int_{\mu_2}^{\mu_1} v_k \frac{dk}{d\varepsilon_k}\frac{d\varepsilon_k}{2\pi} f_1(1-f_2) = \frac{2e}{h}T(\mu_1-\mu_2)$$

where electron's group velocity $v_k = \hbar k/m^*$, e is the elementary charge. In the energy range $\mu_1 \sim \mu_2$, $f_1 = 1$ is the Fermi distribution for the electronic initial state in the left electrode and $f_2 = 0$ is the empty Fermi distribution for the electronic final state in the right electrode. The factor 2 accounts for the spin degeneracy of electrons. Considering $G = I/V$, then

$$G = \frac{2e^2}{h}T$$

when $T(E) = 1$ and N is the number of conductive channels. The conductance is

$$G = \frac{2e^2}{h}N$$

Usually, the conductance of a single-channel perfect wire with spin is called the quantum conductance[54]

$$G_0 = \frac{2e^2}{h} \approx 77.48\ \mu S = \frac{1}{12\,900}\ \Omega^{-1}$$

3. Nanoionics-enabled construction of the APC structures

Nanoionics is an emerging research field focused on the study of ion transport in solid-state nanosystems. It plays a pivotal role in facilitating technological progress, particularly in information technology and energy sectors, where the use of ions as charge carriers has garnered significant attention. In recent years, researchers have successfully demonstrated the construction of APC structures within solid-state nanosystems, which has attracted considerable interest due to its advantages such as high efficiency, reconfigurability, and excellent compatibility with CMOS technology.[25] In nanoionics-constructed APC structures, the electric field is used to control the distribution of ions at the atomic scale, allowing the APC structure to be reconfigured. Specifically, the electric field induces redox reactions and ion migration within the heterojunction, composed of electrode/solid electrolyte/electrode multilayers, thereby forming a nano-conductive channel connecting the top and bottom electrodes. By precisely controlling the dimensions of this nano-conductive channel, APC structures can be constructed, enabling the observation of the quantum conductance effect at room temperature.[56,57]

APC structures can be classified into two principal categories according to the types of migrating ions involved: metallic type and vacancy type. Metallic-type APC structures are typically formed by the migration and redox reactions of active metal cations injected from the electrode. During operation, the electric field induces the migration of metal cations in the solid electrolyte, where they undergo electrochemical reactions to deposit as metallic atoms or clusters, thereby forming conductive channels between electrodes. In contrast, vacancy-

type APC structures are constructed by the formation of vacancies induced by the migration of anions within the solid electrolyte. When anions migrate under an electric field, vacancies are created in the lattice structure. These vacancies can act as effective atomic-scale constrictions, exhibiting quantum conductance effects when they are appropriately controlled. The formation and annihilation processes of both types of APC structures involve complex electrochemical interactions and ion movements within the solid electrolyte. These processes are crucial for developing advanced nanoelectronic devices and exploring quantum phenomena at the atomic level.

3.1. Evolution dynamics of the APC construction

3.1.1. Metallic-type. This phenomenon typically occurs in active metal electrodes (*e.g.*, Ag, Cu, Ni, *etc.*) constructed as heterojunctions with a solid electrolyte dielectric layer.[58,59] When applying an electric field, a metallic APC structure will be formed within the solid electrolyte film, primarily consisting of materials from the active metal electrodes. When a positive voltage is applied to the active metal electrode, the following ion migration and redox reaction processes will occur: (I) an oxidation reaction ($M - ze^- \rightarrow M^{z+}$) takes place at the active metal electrode, and the metal cations (M^{z+}) will migrate towards the counter electrode (cathode) driven by the electric field. At this stage, the conductance of the heterojunction is far below G_0 ($G \ll G_0$) because the APC structures are not fully formed; (II) as the positive voltage continues to increase, reduction reaction ($M^{z+} + ze^- \rightarrow M$) occurs at the cathode, leading to the formation of an APC structure consisting of metal atoms within the solid electrolyte, and the conductance of the heterojunction stabilizes around $G \approx G_0$; (III) with further accumulation of reduced metal atoms at the cathode, the lateral dimensions of the APC expand, forming a nano-conductive channel. Consequently, the conductance of the heterojunction increases significantly above G_0 ($G \gg G_0$).

As shown in Fig. 5a, the schematic diagrams illustrate the redox reaction of Ag^+ and the formation of Ag APC structure within the Ag/polymer/Au heterojunction.[60] Subsequently, a negative bias was applied to the active metal electrode following the establishment of nano-conductive channels. A similar redox process occurs within the metal nano-conductive channel. Metal atoms progressively detach from the nano-conductive channel, leading to a reduction in its lateral dimension. The APC structure gradually thins and completely disintegrates. By alternately applying positive and negative voltages, the metallic APC structure undergoes repeated formation and dissolution, facilitating the reconfiguration of atomic structures. Aono *et al.* fabricated a Pt/nanogap (1 nm)/Ag_2S/Ag heterostructure following this principle, as shown in Fig. 5b. They applied a positive voltage to the Ag electrode, enabling Ag^+ to be reduced to Ag atoms at the nanogap between Ag_2S and Pt. By managing the growth of Ag atom clusters on the surface of Ag_2S under the electric field, the size of the contact could be controlled between Ag atom clusters and the Pt electrode. This controlled process ultimately allowed for the construction of an APC structure.[15] Furthermore, Nandakumar *et al.* designed a SiO_2-based device with a Cu top electrode for the low-temperature back-end-of-line (BEOL) process integration as displayed in Fig. 5c.[61] The device demonstrated a quantized conductance effect, where the lateral dimension of the nanofilament was estimated by modelling a single filament and measuring the voltage drop across the device during conductance transitions. Experimental results revealed that the device displayed quantization conductance at half-integer multiples of G_0 due to the presence of energy sub-bands in the Fermi level split between contact reservoirs. In addition, Yang *et al.* proposed a technique called electrochemically assisted mechanically controllable break junction (EC-MCBJ) to construct APC structures (Fig. 5d).[62] The suspended electrode pairs were first patterned and fabricated on the Si microchips by employing traditional photolithography and wet-etching processes.[62] Subsequently, a new alkaline electroplating solution was employed to create Cu nanocontacts between these electrode pairs. By a continuous electrochemical deposition process, the width of the fabricated Cu nanocontacts was reduced to less than 18 nm, leading to the production of numerous Cu quantum point contacts. Overall, this EC-MCBJ method shows many advantages as a novel approach for constructing atomic-scale devices.

3.1.2. Vacancy-type. The vacancy-type APC structure is similar to that of the metallic-type, both of which are based on the ion migration process and electrochemical reaction. However, the metallic-type APC structure is based on the electrochemical reaction of active metal cations (such as Cu^{2+}, Ag^+, *etc.*), while the vacancy-type is related to the anions (such as O^{2-}, *etc.*) in the solid electrolytes, including V_2O_5, HfO_x, TaO_x, CeO_x, and ZnO.[63]

Here, the detailed formation and dissolution processes of vacancy-type APC structures were illustrated, as shown in Fig. 6a.[64] In this process, inert materials are used as the top and bottom electrodes. When a positive bias is applied to the top electrode (anode), the O^{2-} ions from the solid electrolyte migrate towards the top electrode, resulting in the formation of oxygen vacancies within the solid electrolyte. As these vacancies rearrange, a nano-conductive channel is formed from these vacancies, significantly increasing the heterojunction conductance ($G \gg G_0$). Subsequently, the O^{2-} ions near the nano-conductive channel undergo electrochemical reactions when applying a negative bias to the top electrode, leading to the dissolution of the nanostructure. As the negative bias increases, the lateral dimensions of the nano-conductive channel decrease to form an APC structure. At this stage, the heterojunction conductance stabilizes around $G \approx G_0$. The APC structure is completely broken after further increasing the negative bias, resulting in a small heterojunction conductance ($G \ll G_0$). Similarly, the reconfiguration of the vacancy-type APC structure can be realized under the alternating action of positive and negative voltages.

To gain a deeper understanding of the formation of the structure, the composition and nanostructure of nano-conductive channels are usually verified using transmission electron microscopy (TEM), energy dispersive spectroscopy

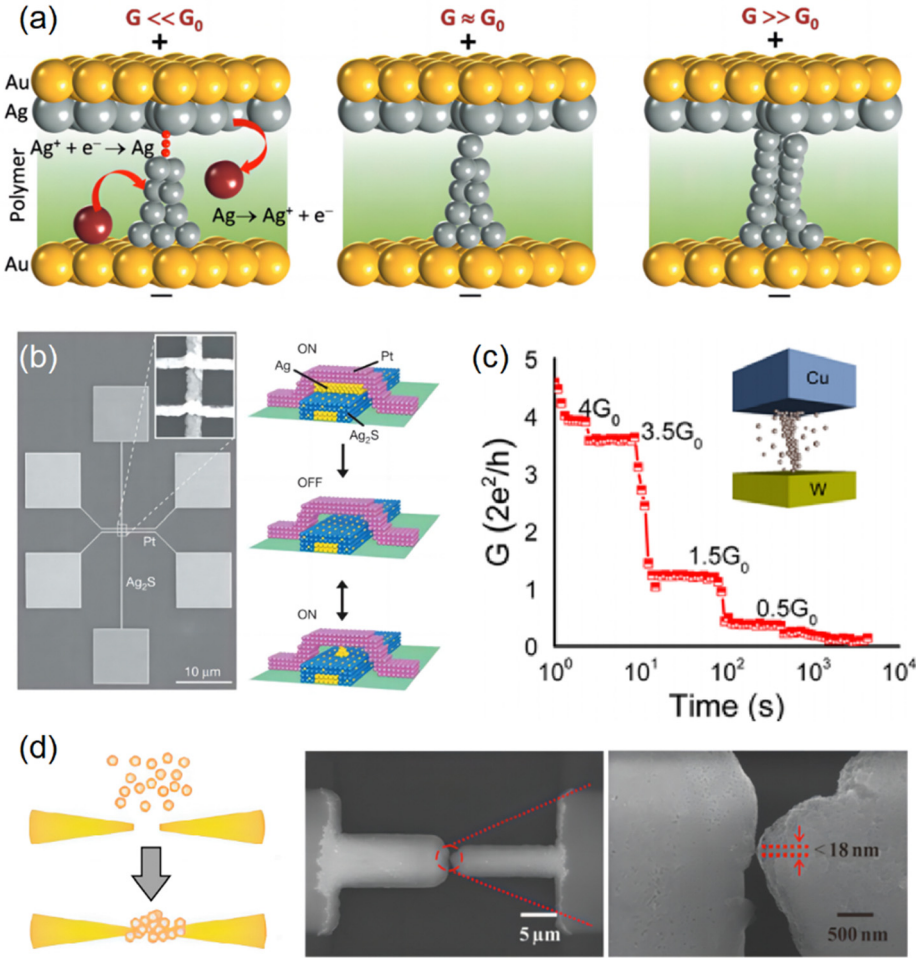

Fig. 5 Metallic-type APC structures. (a) APC structures were constructed through Ag ion migration and electrochemical processes.[60] (b) SEM image and Ag ion migration process of the Pt/nanogap (1 nm)/Ag_2S/Ag heterostructure.[15] (c) APC structures and quantum conductance effects in the Cu/SiO_2/W device based on Cu ion migration.[61] (d) The fabrication of the APC structures through an electrochemically assisted mechanically controllable break junction (EC-MCBJ) method.[62]

(EDS), and other analysis methods. For example, Xue *et al.* employed high-resolution TEM (HRTEM) to analyze partially and fully formed oxygen vacancy conductive filaments.[65] Their study demonstrated that 32 discrete quantum conductance states could be repeatedly tuned by controlling the O^{2-} ion migration. The dissolution process of atom-sized oxygen vacancy filaments within the Pt/HfO_x/ITO structure was also observed using voltage pulses (Fig. 6b). Furthermore, Peng *et al.* selected HfO_x as the solid electrolyte and constructed a TiN/Ti/HfO_x/TiN valence-change device,[66] which was analyzed under a HRTEM, as shown in Fig. 6c. The appearance of half-integer multiples of G_0 instead of only integer multiples could be attributed to several factors, including differences in chemical potentials between the two carrier reservoirs along the filament, reconfiguration of atomic contacts, and the potential impact of weak magnetism due to oxygen vacancies. With carefully controlled conditions, a stepwise decrease in conductance from 9 to 0.5 G_0 in steps of 0.5 G_0 could be successfully achieved using pulse-mode reset procedures. These experimental results underscore the importance of monitoring the measured bias voltage to evaluate the quality of the device preparation and measurements employed in the study of conductance quantization, which will facilitate future advancements in device design and fabrication.

Both metallic and vacancy-type APC structures have been successfully constructed in various solid electrolytes, including polymeric materials, metal oxides, metal sulfides, two-dimensional (2D) graphene, and silicon dioxide materials. A comparative analysis of these two types of APC structures shows that their stability is significantly influenced by the ion migration activation energy. Higher migration activation energy reduces spontaneous ion diffusion, thereby enhancing the stability of the APC structures. Typically, the O^{2-} ions in the oxide medium exhibit higher migration activation energy compared to Ag^+, Cu^{2+}, and other active metal ions. For example, the migration activation energy of O^{2-} ions in ZnO is approximately 2.4 eV, while for Ag^+ and Cu^{2+} ions, it is only 0.9 eV and 1.4 eV, respectively. Thus, vacancy-type APC structures offer better control and stability of quantum conductance states than metallic-type APC structures. Moreover, statistical analyses

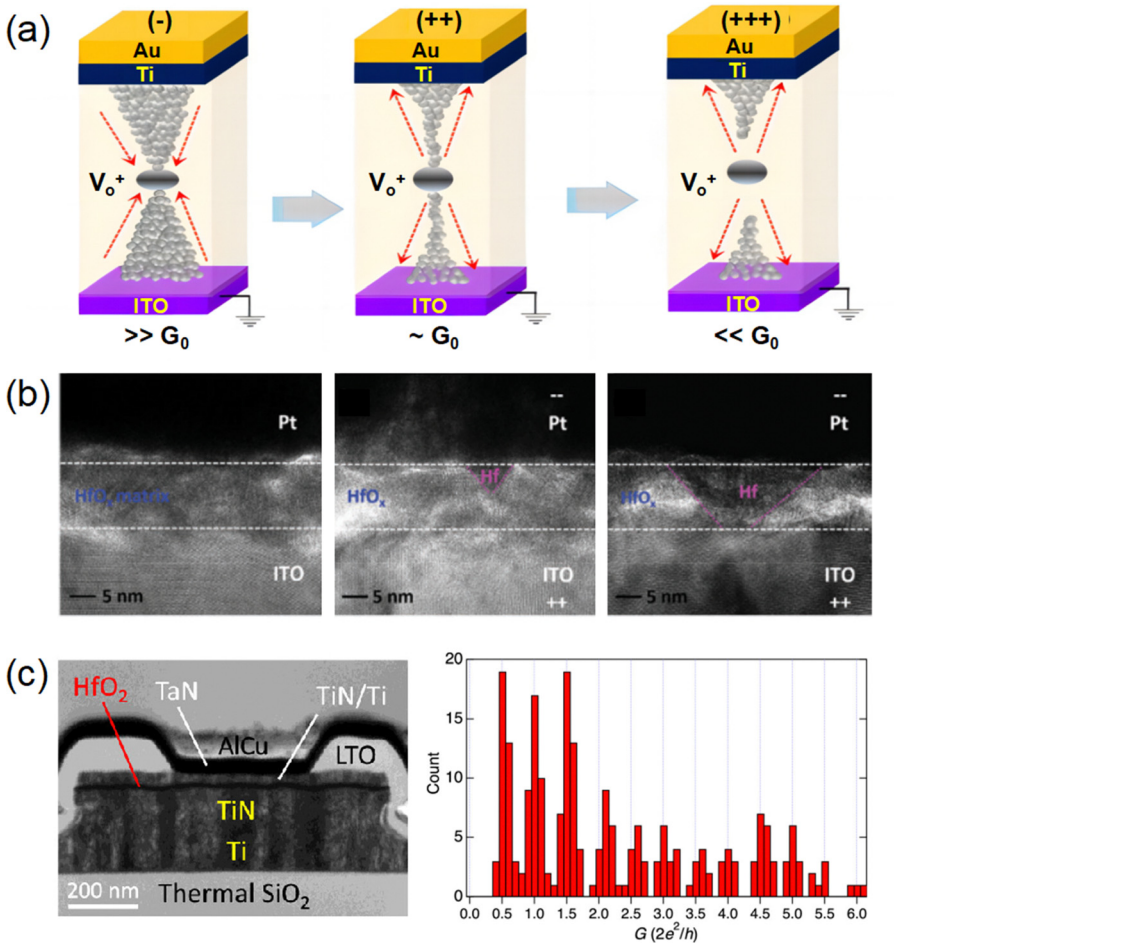

Fig. 6 Vacancy-type APC structures. (a) APC structures were constructed through oxygen ion migration and electrochemical processes.[64] (b) HRTEM images of the partially and fully developed oxygen vacancy conductive filaments.[65] (c) TEM image of the cross-sectional view of the TiN/Ti/HfO_x/TiN device. Histogram of conductance plateau values retraced from 330 reset operations.[66]

show that vacancy-type APC structures tend to exhibit quantum conductance with both integer and half-integer multiples of G_0, whereas metallic-type structures are more likely to display conductance in integer multiples of G_0.[56] This difference may be attributed to the inherent conductance properties of the two types of structures. As a result, vacancy-type APC structures are more suitable for achieving higher-density storage. Furthermore, due to the higher migration and activation energies of vacancies, vacancy-type APC structures typically require a higher driving voltage to maintain better stability.

3.1.3. Low-dimensional materials. Investigating the behavior of quantum conductance is significant and holds promise for diverse applications. Unlike traditional bulk materials, low-dimensional materials exhibit distinctive quantum effects due to their reduced dimensions, such as the quantization of electron wavefunctions and tunneling phenomena, which profoundly influence quantum conductance.[67] Moreover, the observation and measurement of quantum conductance in low-dimensional materials are more accessible through experimental techniques. As a result, low-dimensional materials provide an ideal framework for studying quantum conductance, attracting considerable interest in scientific research. Metallic nanowires constitute a novel class of one-dimensional (1D) conductive materials that combine the outstanding electrical conductivity of metals with the unique size-dependent properties of nanomaterials. These nanowires hold significant promise for applications in electronic device technologies. The above-mentioned MCBJ,[68] STM,[69] and TEM approaches[41] are commonly utilized to fabricate one-dimensional atomic chains and explore their electrical characteristics. Generally, 1D metallic nanowires display strong light scattering and trapping abilities, which enhance light absorption.[70] Carrier mobility within one-dimensional nanowires is predominantly confined along the axial direction, resulting in increased carrier mobility and improved performance in nanodevices.

Recently, Emboras *et al.* engineered 1D Ag atomic chains within heterojunctions that exhibited memristive characteristics, effectively integrating electrons and photons.[71] By utilizing the interplay between electrons and photons to manipulate the APC structure, they realized ultra-sensitive photodetection at the atomic scale, as depicted in Fig. 7a. Under the electric field,

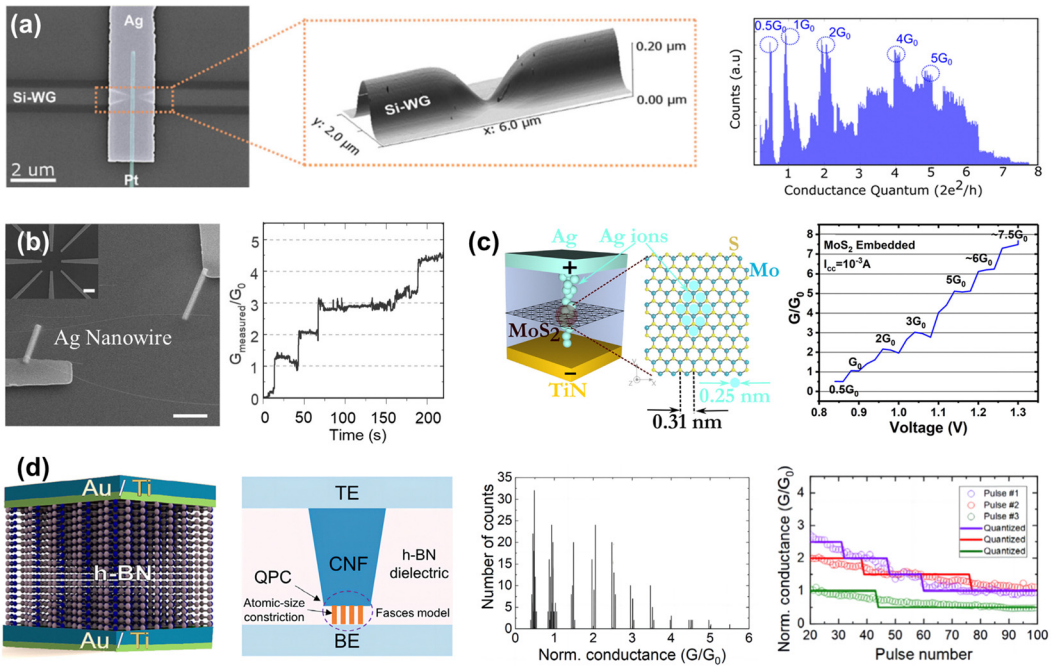

Fig. 7 Quantum conductance of APC structures in (a) and (b) 1D and (c) and (d) 2D materials. (a) SEM picture of the atomic photodetector. The atomic force microscopy image of the device before the deposition of the metals and a vertically oriented 3D waveguide tip (left). Histogram of optically induced conductance quantization (right).[71] (b) SEM image of a single nanowire device obtained by connecting an Ag nanowire to a pre-patterned electrode using IBID deposition of Pt contacts (scale bar, 10 mm). The inset shows a low-magnification SEM image of the pre-patterned sub-millimetric probe circuit (scale bar, 50 mm). Quantum conductance effect in the nanowire device.[72] (c) Quantum conductance effect in the Ag/SiO_2/MoS_2/SiO_2/TiN structure with 2D MoS_2-embedded in the device and quantum conductance of the device after applying a DC bias of 1.3 V.[73] (d) Schematic of the memristors fabricated using an h-BN dielectric and histogram of the normalized conductance.[74]

Ag atoms undergo migration and redox reactions, leading to the lateral diffusion of Ag ions and the formation of conductive filaments. The elevated optical signal power may locally heat the system, thereby amplifying the electrochemical processes and modifying the structure of the conductive filaments, generating the APC structure. Furthermore, a histogram covers conductance values ranging from a fraction of G_0 up to multiples. Visible peaks appear around integer multiples of G_0 (1, 2, 4, and 5 G_0), indicating that the fabricated Ag-α-SiO_2-Pt device operates at the atomic scale and involves the relocation of only a few atoms. The slight deviations observed in conductance from integer values of G_0 are attributed to contact resistance effects, as well as defects and impurities at the Ag/Pt interface, which cause electron wave scattering and energy loss. Besides, Milano *et al.* investigated the morphological transformations of individual Ag nanowires with memristive properties during breakdown as shown in Fig. 7b.[72] *In situ* scanning transmission electron microscopy (STEM) measurements were conducted to observe the detailed process. Molecular dynamics simulations revealed four distinct stages in the dynamic evolution of conductive filaments: (I) the migration of Ag atoms along the edges of the nanowires under the influence of an electric field; (II) the nucleation and subsequent growth of Ag atoms; (III) the formation of Ag conductive filaments bridging the nanowire ends; and (IV) the lateral expansion of these Ag conductive filaments. This comprehensive analysis provided deeper insights into the mechanisms that govern and regulate ion transport in APC structures.

Quantum conductance is generated through the formation of atom-level conductive channels. The 1D materials provide significant dimensional advantages in constructing the APC structures through simple mechanical stretching. As bottom-up building blocks, 1D structures provide key benefits such as ultimate scalability, high spatial localization of switching events, and a large surface-to-volume ratio, which can be harnessed to modulate electronic and ionic transport properties. The varying Schottky barriers between nanowires and electrodes in these devices enable self-limited currents, reducing the risk of Joule heating.[75] Furthermore, short-term plastic effects can be modeled using the enhancement–inhibition rate balance equation commonly seen in ion transport kinetics.[76]

Over the last few years, 2D nanomaterials have garnered significant attention due to their distinctive physical and electronic properties, holding great promise for advanced electronics. Many nanodevices now incorporate solid-state or 2D materials as dielectric layers in vertical structures, where the active layer is sandwiched between two electrodes.[77] In such designs, the APC structures are typically formed by ion migration through the 2D material dielectric layer under the influence of an electric field. The wide variety of available 2D materials offer extensive options for constructing APC structures. By exploring the interaction mechanisms between ions

and these materials, advanced nano-ionic devices have been designed and fabricated.[78,79] Furthermore, the atomic-level thickness of 2D materials and the weak van der Waals forces between layers contribute to their exceptional potential in electronics, providing superior downscaling capabilities, easy stackability, and compatibility with traditional silicon-based devices.[80]

In previous works, memristors have usually been fabricated using bulk materials and constructed into a sandwich structure, where electric fields facilitate the transport of active ions and the formation of APC structures. The quantized conductance observed in these devices arises from the minimal size of the APC structures, leading to resistive switching phenomena. 2D materials have potential as alternative materials for sandwiched memristor devices because of their many merits. As illustrated in Fig. 7c, Kitsios *et al.* investigated the resistive switching behavior of a thin SiO_2 layer embedded with 2D MoS_2 in a conductive bridge random access memory (CBRAM) configuration.[73] The device demonstrated enhanced conductance quantization, exhibiting eight distinct quantized conductance states during direct current (DC) operation, which increased to 10 states under pulse measurements. To further understand the mechanism, the kinetics of Ag in relation to the recorded variability was studied. It was observed that the presence of MoS_2 thin films induces a sieving effect, confining Ag atoms as they traverse the films, thus limiting the conductive channel during its formation. Consequently, the diameter of the conductive channel approaches that of a quantum wire structure. As Ag atoms pass through multiple layers of MoS_2 thin films, they exhibit a dendritic morphology, leading to the formation of multiple conductive channels and fluctuations in variability. This condition also affects quantum conductance, leading to the manifestation of non-integer values.

Quantum conductance can realize multifaceted operations, significantly enhancing both efficiency and precision. Besides regulating ion transport to establish APC structures within the 2D MoS_2, the hexagonal boron nitride (h-BN) has an atomically smooth surface free of dangling bonds and remarkable tensile strength,[81] showing great potential applications. These characteristics make h-BN highly compatible with CMOS circuits and flexible switching devices. Roldan *et al.*[74] fabricated an Au/Ti/h-BN/Ti/Au device using h-BN as a dielectric layer. The vertical control of the APC structure was achieved through the regulation of ion transport and redox reactions under an electric field as presented in Fig. 7d. By employing the quantum point contact model to analyze obtained experimental data, it was found that the resistance of the device increased as the number of channels decreased during the reset process. Initially, a significant decrease in current was observed in the pulse train, but it eventually saturated, corresponding well with quantized conductance values. The normalized conductance (G/G_0) tends to converge to half-integers or integers. This procedure was repeated for all pulse trains, and a resultant histogram was computed, revealing observable conductance quantization.

2D materials encompass a variety of semiconductors and insulators. Unlike traditional oxides with thicknesses of just a few nanometers, 2D materials have periodically arranged lattices, allowing them to function as atomic sieves that control ion diffusion barriers and lead to more stable APC structures. Additionally, 2D materials can form heterojunctions with other materials, where the interlayer coupling strength can be modulated by van der Waals forces. This modulation facilitates the construction of high-quality APC structures across different materials. Furthermore, the diverse band gap characteristics of 2D materials provide better control over quantum tunneling effects, offering a pathway to generate multiple quantum conductance states.

3.2. First-principles calculations of nanoionics enabled APC structures

Since DFT cannot be applied to open systems and is not a non-equilibrium theory, Taylor *et al.* established the first-principles calculations by DFT within the framework of nonequilibrium Green's function (NEGF) theory to address the above issues and produced the quantum transport package McDCal.[82] Over the past few decades, the NEGF method has been developed to investigate and predict the transport properties of nanoscale materials, as well as the operation and performance of nanoscale devices.[83] The implementation of transport theory has been combined with existing computing software for electronic structures, *e.g.* Nanodcal,[82] TranSIESTA,[84] SMEAGOL/Gollum,[85] GPAW,[86] Atomistic NanoTransport,[87] ASE,[88] ATK.[89] The electric current can be evaluated using the Landauer–Buttiker formula:[55]

$$I = \frac{2e}{h}\int_{\mu_1}^{\mu_2} \mathrm{d}E T(E)(f_1(E) - f_2(E))$$

Here, f_1 and f_2 denote the Fermi distributions in the left and right contacts, respectively

$$f(E-\mu) = \frac{1}{1 + e^{E-\frac{\mu}{k_B T}}}$$

where k_B represents the Boltzmann constant, T represents the temperature, μ_1 and μ_2 represent the chemical potentials of the left and right electrodes, respectively. The transmission function $T(E)$ represents the probability weight for a particle to be transmitted when it approaches the APC structure with energy close to E

$$T(E) = \mathrm{Tr}[\Gamma_L(E) G^r(E) \Gamma_R(E) G^a(E)]$$

where G^r and G^a are the retarded and advanced Green's functions with Γ_L and Γ_R as the coupling functions of left and right electrode self-energies, respectively.

At present, the calculated conductance and I–V curves of the APC structure can be obtained by examining the transport properties from the transmission spectra at the zero or continuous bias voltage based on the first-principles electron transport simulation, DFT+NEGF method.[90] For example, the APC structure of metal ions in Ag/PEO/Pt devices exhibited

reproducible quantized conductance $\sim 1\ G_0$ in *I–V* measurements. A symmetric three-atom chain with different numbers of Ag atoms in the channel region was constructed to explain the experimental observations. The calculated conductance of single-atom (two-atom) point contact was ~ 1 (2) G_0 and dropped quickly to $< 1\ G_0$ when extending the tunneling gap (Fig. 8a).[91] Besides, ordered vacancy filaments of atomic thickness can form a transmissive channel between two metal contacts, which can also exhibit quantized conductance.[92] By removing the adjacent oxygen atoms in HfO_2, a metallic oxygen vacancy (V_o) filament penetrates the entire oxide film (Fig. 8b),[93] and the calculated conductance values are 1.02 and 1.13 G_0, consistent with the experimental distribution of the conductance of the intermediate states, which has a peak at 1 G_0.[94] When an oxygen atom moves into the filament, the conductance decreases exponentially. With the oxygen at the fourth oxide layer, the conductance becomes two orders of magnitude smaller than the open V_o filament. Along with one oxygen atom moving from position 5 to the center (position 8), two one-dimensional potential wells of V_o filament in 15 HfO_2 layers become identical, and the conductance increases quickly from 10^{-3} to 0.31 G_0 for the resonant transport. The resonant tunneling of the discontinuous vacancy filament could significantly alter the magnitude of quantum conductance, which provides an idea for the use of single atom control to realize resistance change based on the conductive mechanism of oxygen vacancies.

Beyond the APC structures derived from manual construction or experiments, molecular dynamics (MD), based on Newton's laws of motion, can provide complex structures that change continuously over time. Subsequently, the quantum transport simulations can investigate the correlation between observed integer multiples of the fundamental quantum conductance and distinctive dynamic trajectories of filament atomic reconfiguration. By EchemDID MD,[96] the external voltage effect is considered by changing the electronegativities of the atoms in the bottom and top electrodes. To simulate the rewriting process of Ag nanowires (Fig. 8c), typical atomic configurations extracted during filament evolution obtained from MD results are used to calculate the transmission coefficient T, where $T = G/G_0$.[72] The calculated conductance is close to 0 G_0 before the conductive filaments are connected (structures 1 and 2). As the conductive filament thickens, the conductance gradually increases from 1 to 4 G_0 (structures 3–6). The quantized conductance, referring to electrochemical processes and ionic dynamics, has been reproduced by quantum transport simulation, which would deepen the understanding of the relationships between the geometric shapes of nanofilaments and quantum conductance in APC structures.

The changes in quantum conductance in the filament formed by the injection of active metals into the dielectric material can also be modelled by first-principles methods. In the monolayer MoS_2, the adsorption of metal ions in the point defects of the 2D layer can explain the resistance switching mechanism from the HRS to the LRS.[97] As shown in Fig. 8d, a MoS_2-based bilayer metal–insulator–metal (MIM) device was built, where grain boundaries existed in the middle of the MoS_2 layers.[95] At 0 V, the device remained in the HRS with slight changes. As the voltage increases, the surface Au atoms dissolve due to the difference in charge. At a certain voltage, the atoms in the electrodes start to move through the grain boundary. As the voltage increases, more Au ions move into the grain boundary, forming a conductive filament. The device switches to the LRS when the Au ions connect the two electrodes. Furthermore, a model of two layers of MoS_2 and four Au layers on both sides was also built for electron transport calculations, which showed that the conductivity increases with the number of Au atoms, from ~ 2.8 to $\sim 4.1 \times 10^{-4}$ S (about 4–5 G_0). Adding less than 5 Au atoms to the grain increases the conductance slightly because the Au atoms have not created a conductive path. As the number of Au atoms increases from 5 to 24, the conductive filaments form and thicken, causing the conductance to change. When the number is increased to 30, the conductance saturates as the filaments become sufficiently thick. The calculation demonstrates how the conductance evolves during the formation of conductive filaments.

4. Modulation of the quantum conductance in APC structures

The intricate atomic-level structure of atomic point contact (APC) structures, composed of a minimal number of atoms, makes them highly sensitive to applied physical fields that influence their quantum conductance states. Previous studies have shown that electric and magnetic fields can alter electron energy levels and tunneling probabilities.[98] In addition, the stress field can modulate the atomic spacing and lattice structures, thereby optimizing the electron transport pathways.[99] Temperature gradients can induce thermoelectric effects and thermoelectric conversion, further influencing conductance behavior.[100] Therefore, the dynamic regulation of quantum conductance through these multi-physical field approaches will enhance the functionality and flexibility of devices, paving the way for the development of high-performance, low-power quantum information devices.

4.1. Quantum conductance modulation under non-electric fields

Multiple external physical fields have been used to modulate the quantum conductance effects. Recently, Zhang *et al.*[13] reported an atomic-scale metallic contact structure by precisely stretching an Au wire. They employed a commercial light-emitting diode (LED) lamp as the light source to adjust the quantum conductance of the constructed APC structure (Fig. 9a). The conductance increased from 10^{-5} to 80 G_0 with a delay of 1–2 s upon light stimulation. Conversely, the conductance decreased to below 1 G_0 after the light was turned off. As depicted in Fig. 9a, the localized plasmon resonances of the nanogaps resulted in significant light absorption in the visible and near-infrared region, involving quantum tunneling effects.[101,102] The absorbed light was converted into thermal

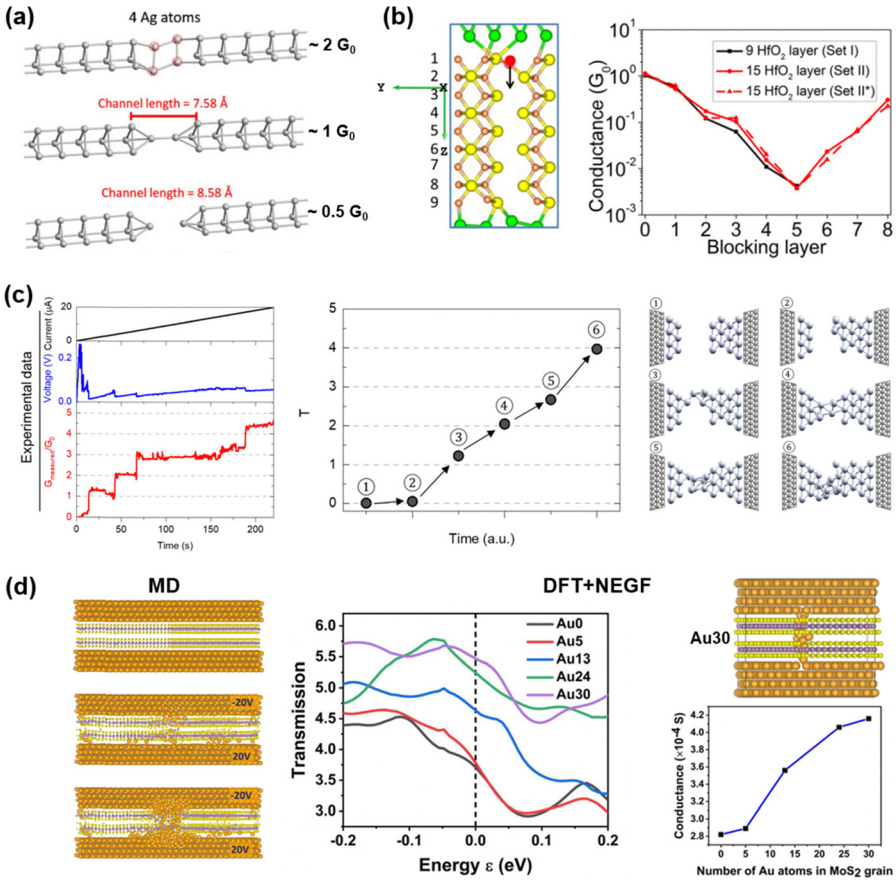

Fig. 8 First-principles simulation of quantum conductance. (a) Atomic configuration of a three-atom chain with single-atom (two-atom) point contact and tunneling gap.[91] (b) Optimized atomic structure of a Pt/9-layer HfO_2/Pt device and evolution of the device conductance as an oxygen atom blocks the V_o filament at different atomic layers.[93] (c) Quantum conductance effects in a current sweep-induced nanowire rewiring, and evolution of the transmission coefficients and atomic structures during the rewiring process computed by DFT simulations.[72] (d) MD simulation of Ag migrating in multilayer MoS_2, plot of zero-bias transmission spectra calculated for device configurations, the structure of 30 Au (Au30) atoms placed randomly inside the grain boundary regions of MoS_2, and the change in electrical conductance with the number of Au atoms in MoS_2 grains.[95]

energy, causing the nanoelectrodes to expand and reconnect. When the system achieved thermal equilibrium, the conductance reached its maximum value. As the light intensity diminished, the metal wire stretched due to electrode shrinkage, resulting in the separation of the electrodes once more after the light was fully extinguished.

The thermal expansion effect induced by light fields in metal nanowires allows for the reconstruction of the APC structures, enabling precise control over changes in conductance states. Since electrons act as carriers for both heat and electric current, electrical and thermal conductance in metals are interconnected at the macroscopic scale.[105] Exploring thermal transport in atomic-dimensional junctions is essential for grasping the quantum phenomena of energy transmission.[106,107] Köymen *et al.*[103] explored the relationship between quantum conductance properties and temperature for Cr/Au/TiO_2/TiO_x/Cr/Au memristive devices as presented in Fig. 9b. Nonlinear behavior in the current–voltage (*I*–*V*) characteristics could be observed due to the insulating nature of TiO_2 and the presence of inversely polarized Schottky barriers at the metal–insulator interfaces as the ambient temperature decreases from 290 to 18 K in the pristine device. Their analysis confirmed that resistance increases with decreasing temperature, both in the pristine state and in resistance states approaching the quantum conduction regime. In addition to temperature, external magnetic fields also affect the quantized conductance values in the APC structures. Strontium titanate ($SrTiO_3$), a perovskite oxide known for its electrostatic tunability, superconductivity, and spin–orbit coupling, shows promise for the development of quantum device. However, exploring quantum effects in $SrTiO_3$ nanostructures is challenging because of inherent disorder. Mikheev *et al.* reported high-mobility, gate-tunable devices based on $SrTiO_3$ with a thin hafnium oxide (HfO_x) barrier layer, as shown in Fig. 9c. These devices demonstrated ballistic constrictions and precise quantization of conductance in the normal state.[104] The presence of a magnetic field caused a sequence of subband degeneracies due to electron mass anisotropy. The analysis of the first conductance step in line traces of G revealed that the twofold degeneracy of this step persisted up to a magnetic field of approximately 7 T. Beyond this, the twofold degeneracy was broken, and the magnitude of the first

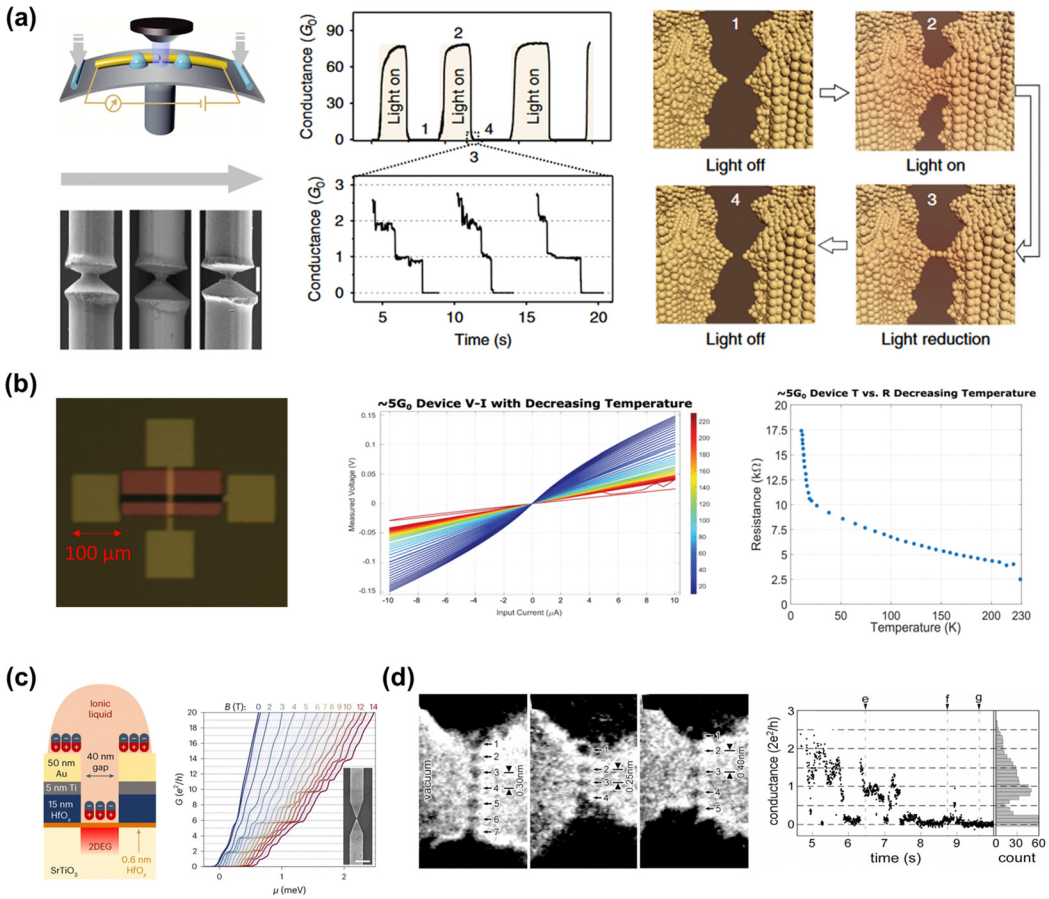

Fig. 9 Impact of various physical fields on quantum conductance. (a) A schematic representation of the atomic-scale metallic contact using the MCBJ technique, and SEM patterns of the notched microwire during the stretching process (left). Real-time measurement of the current with the light switched on/off and the corresponding conductance values as the light intensity changes (middle). Schematic of the atomic arrangement, which corresponds to four conductance states upon light illumination (right).[13] (b) Microscopic image of the Cr/Au/TiO_2/TiO_x/Cr/Au device (left). The *V*–*I* plot and variation of resistance with current input and decreasing temperature when the device is set to 5 G_0.[103] (c) Schematic cross-section of the constriction region. The red and blue dipoles represent the polarized layer of ionic liquid molecules (left). Zero-bias conductance *G* as a function of gate voltage (converted to chemical potential μ), with magnetic field B tuned between 0 and 14 T (right).[104] (d) HRTEM images of Au ASWs showing the average interatomic distance (0.30 nm), minimum interatomic distance (0.25 nm), and maximum interatomic distance (0.40 nm). Contact conductance during the tensile deformation as a function of time and the corresponding histogram.[99]

few conductance steps became half of G_0 at higher magnetic fields.

Understanding the role of strain in modulating conductance is crucial for analyzing the effects of various mechanisms on conductance. Previous studies have demonstrated that strain can significantly impact ballistic conductance. For example, Hossain *et al.*[108] revealed that in a graphene-based device, applying uniaxial compression to the graphene sheet within a lead–graphene-lead configuration maintains its unstrained ballistic conductance properties for electrons with energies exceeding the system's Fermi energy threshold. In contrast, for all other strain conditions, regardless of the electron energy, graphene's ballistic conductance will either increase or decrease depending on the specific type of strain.

For Au nanometer-sized contacts, the conductance decreases in a stepwise manner during the thinning process, with each conductance level corresponding to approximately integer multiples of G_0.[109] Kizuka explored the fluctuation in atomic configuration during the formation of Au APC structure through the integration of *in situ* HRTEM with conductance and force measurements (Fig. 9d).[99] Notably, the APC structure comprising five atoms exhibited a stable conductance state of 1 G_0, despite fluctuations ranging between 0.1 and 1.5 G_0. However, a reduction in conductance below 0.1 G_0 was observed as the number of atoms exceeded five. These findings provide compelling experimental evidence for the atomically localized structures in APC systems and reveal a direct correlation between these structures and their mechanical and electrical properties.

4.2. Quantum conductance modulation under the electric field

The electric field plays a pivotal role in the modulation of the APC structures. Particularly, the quantum conductance effects induced by nanoionics are strongly influenced by the underlying ionic electrochemical and dynamic processes under the

electric field. It has been shown that the shape of the atomic-sized contact and the growth direction are determined by the interplay between the electrochemical reaction rate and ion mobility within the solid electrolyte.[110] These factors can be effectively controlled through various parameters such as driving forces (*e.g.*, current or voltage sweeps), compliance current (I_{cc}), stop voltage, and sweep ramp rates. Consequently, these controls allow for precise modulation of the corresponding quantum conductance levels.

The influence of driving forces on quantum conductance effects, such as current and voltage sweep stimulation, has been widely explored. Köymen *et al.* applied slow current and voltage inputs in the Cr/Au/TiO_2/TiO_x/Cr/Au devices during the formation and annihilation processes of the APC structure, respectively.[103] They applied slow current and voltage inputs and simultaneously monitored the current–voltage trends, observing quantum conductance steps induced by these electrical inputs. Additionally, a detailed statistical analysis of the quantum conductance effects was conducted for both methods. Current sweep stimulation caused step-like changes in the measured voltage, corresponding to the formation of APC structures and resulting in discrete steps in device conductance. More readily and frequently distinct integer conductance levels could be achieved, which is mainly related to the current-enhanced stability effects involving the interplay between surface tension and quantum pressure forces on the APC structure. This phenomenon has also been reported in other traditional MIM heterojunctions based on thin films with Ag electrodes and in single metallic nanowires such as Ag.[111] During voltage sweep stimulation, both distinct integer and half-integer conductance levels were detected, achieving a wider range of quantized conductance states.

Experimental results indicate that quantum conductance levels can be accurately modulated by appropriately tuning the programming parameters. For example, a higher I_{cc} of 400 μA was used to obtain 2.5 G_0, while lower conductance levels of 1 G_0 can be achieved by reducing the I_{cc} to 100 μA.[72] Zhu *et al.* reported a similar approach for quantum conductance regulation, achieving a monotonic increase in conductance states.[112] They first achieved a quantum conductance state of 2.5 G_0 with an I_{cc} of 100 μA, which then increased to 4.0 G_0 with an I_{cc} of 250 μA, followed by 4.5, 6.5, and 8.5 G_0 with further enhanced I_{cc} values. This is because the higher I_{cc} tends to generate a strong and thick APC structure, which allows more sub-bands for electron ballistic transport. Notably, similar quantum conductance levels can be realized with different I_{cc} values across various devices or even with the same structure. Besides, a similar behavior was also observed in the annihilation process of the APC structure by controlling the stop voltages. For instance, the initial conductance of the device was first switched to 20 G_0 and then several distinct quantum conductance levels of 2, 1.5, 1, and 0.5 G_0 can be obtained as the stop voltage increases.[26]

4.2.1. Stability. The quantum conductance effect produced by the APC structures offers a promising direction for the miniaturization of information devices. Achieving a stable quantum conductance state is important for advancing its practical application. As illustrated in Fig. 10a, the stability of quantum conductance states was estimated in a memristor device employing a Mott insulator-vanadium dioxide (VO_2) configuration with a first-order structural transition. The APC structure was built in an Au/VO_2/NSTO (Nb-doped $SrTiO_3$) device prepared by Zhao *et al.*,[113] with the VO_2 crystals serving as the functional layer oriented along the [120] direction. Due to the grain boundaries within VO_2, oxygen vacancies are confined to narrow grain boundaries owing to significant migration barriers during the migration process. These grain boundaries typically exhibit a size of approximately 1 nm, closely approaching the atomic scale. Meanwhile, it was observed that varying the reset scan voltages leads to the attainment of different conductance states. The jump values of the quantum conductance are concentrated at both integer and half-integer positions of G_0. To assess the retention of quantum conductance states at room temperature, experiments were conducted on states ranging from 0.5 to 5 G_0, with all resistive states remaining stable for up to 2×10^4 seconds.

4.2.2. Endurance. Endurance refers to the ability of devices to withstand long-term and repeated usage under normal conditions and assesses the reliability and stability of the device over a certain period of time. By optimizing the materials selection and device structure design, as well as the suitable electric field modulation, the endurance of the devices can be greatly improved. Switch uniformity is a critical metric for determining the practical viability of a device. The operational failure in threshold-switching devices often arises from the overgrowth of a conductive filament, several atoms thick, caused by excessive diffusion of active metal ions within the switching layer.[102] Hence, it is essential to develop methods to control conductance quantization near the APC structure to effectively modulate the performance of threshold-switching devices. The h-BN is emerging as a promising candidate for resistive switching devices owing to its exceptional properties, including intrinsic insulation and a wide indirect bandgap of about 6 eV.[115] Nikam *et al.* reported a single-atom APC switch using atomically thin h-BN. As shown in Fig. 10b, the device structure consists of a single layer of h-BN (about 0.33 nm thick) sandwiched between two electrodes, forming a single APC structure.[114] The spontaneous fracture of the single-atom filament within this structure can yield remarkable threshold-switching characteristics. As a result, the device has the potential to function as a quantum conductance atomic threshold switch. Moreover, a programmed voltage pulse, characterized by an amplitude of 1 V and a width of 1 μs, was employed to assess the durability of the device during repeated write and wipe operations. The device exhibited a high endurance ($>10^7$ cycles) with no apparent degradation. The cumulative probability distribution of the cycle period and device–device threshold voltage suggests the presence of a stable single-atom APC switch within the atomically thin h-BN, as depicted in Fig. 10b (right).

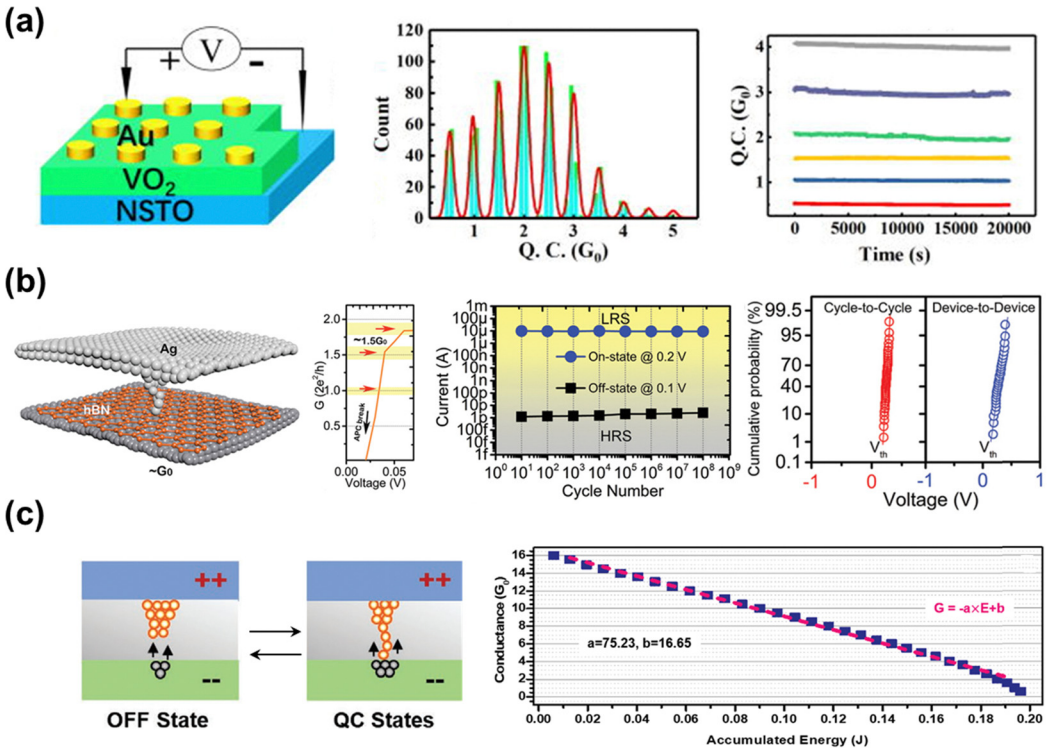

Fig. 10 Performance optimization of quantum conductance in APC structures. (a) Schematic of the Au/VO_2/NSTO device structure with Nb-doped $SrTiO_3$ (NSTO) as the substrate and the bottom electrode (left). Histogram of quantum conductance at 50 reset point cycles (middle). Polymorphic holding properties of quantum conductive states (right).[113] (b) Schematic of a single-atom point-of-contact switch device and quantized conductance states (left). Endurance test using a voltage pulse with an amplitude of 1 V and a width of 1 μs (middle). Cumulative probability of threshold voltage in cycle-to-cycle (red) and device-to-device (blue) measurements (right).[114] (c) Schematic of controlled APC structure evolution *via* oxygen ion migration in an asymmetric Pt/HfO_x/ITO device (left). Conductance *versus* cumulative device energy (right).[65]

4.2.3. Controllability. Polymorphism represents an enticing property in quantum conductance devices, as it allows for more precise regulation. If the polymorphic characteristics associated with quantum conductance effects can be reliably modulated, it would mark a significant advancement in achieving controlled manipulation at the atomic level. In this context, Xue *et al.* fabricated an energy-driven Pt/HfO_x/ITO structure involving single-atom horizontal oxygen manipulation during reduction.[65] Fig. 10c shows a conductance histogram obtained from 778 reset operations conducted across 15 devices. The results revealed that the conductance ranges from 0.5 to 16 G_0, with a concentration observed at integer multiples of 0.5 G_0. This distribution led to the identification of 32 quantized conductance states. A linear relationship between the electrical pulse energy and conductance state indicated a direct correlation between energy input and conductance modulation. This suggests that the continuous quantized conductance modulation was due to the precise energy input applied within the HfO_x insulating layer, driving oxygen migration and electrochemical processes during the reset operation. The observed 32 quantized conductance states in this work confirm the significant potential of resistive change devices in realizing polymorphism. However, achieving tunable polymorphism remains a challenge, and further exploration is needed to develop novel strategies and advance the understanding in this field.

5. Applications

To date, the APC structures have been constructed using a variety of materials and configurations, showing significant potential for the design and manufacture of information devices. These unique structures enable controllable electron transport at the nanometer scale and facilitate the creation of highly integrated and miniaturized electronic devices. Moreover, the APC structures allow for the control of single electrons and precise quantum states, enhancing the operating accuracy and stability of devices. By reducing resistance and energy loss through quantum tunneling, APC structures improve energy efficiency and reduce power consumption. The quantum conductance generated by electrons passing through the APC structures also offers numerous advantages in the information field. It enables charge transport at discrete energy levels, reducing scattering effects and increasing conductivity efficiency. The discrete energy level characteristics of quantum conductance minimize energy loss. Related devices based on quantum conductance also exhibit fast response, which boosts

the speed of information processing. Quantum conductance transmission accommodates thermal noise and other forms of electronic noise, improving signal clarity and reliability. These properties enable efficient information processing that surpasses the capabilities of classical computing. These advantages suggest that quantum conductance provides broad application prospects for future high-performance, low-power information devices. The applications of quantum conductance in the APC structures in different fields are described in detail below.

5.1. Memory

The multilevel quantum conductance generated in APC structures can be utilized for multilevel data storage and the construction of logic circuit elements, offering advantages such as high density, low power consumption, and fast response speed. This is significant for achieving high-density information storage and logic operations. Leveraging quantum conductance enables the design of novel storage devices and computing modes, which creates great development space for information technology. Krishnan *et al.*[116] incorporated the Ag salt into a polyethylene oxide (PEO) film to create a solid polymer electrolyte (SPE). This SPE was then placed between electroactive Ag and Pt electrodes to form a MIM structure, as depicted in Fig. 11a. The resulting device exhibited favorable resistance transition characteristics, earning the moniker 'gapless-type atomic switch'. The resistance of the nanogap between the two electrodes fluctuates as wires are formed and broken. When subjected to an electric field, Ag atoms within the Ag/PEO/Pt devices undergo redox reactions and migrate within the polymer. This migration exhibits a highly controllable and reproducible quantized conductance behavior, confirming the well-controlled formation of the internal APC structure. The statistical histogram of conductance states reveals a distribution ranging from 1 to 10 G_0 under voltage scanning, with prominent peaks observed at both integer and half-integer multiples. Specifically, the conductance states of ≥ 2 G_0 exhibited a certain retention time; the retention time became longer for higher conductance values and is likely to increase exponentially with increasing conductance values. The maximum retention time of $\sim 1.9 \times 10^3$ s was achieved for ~ 9 G_0. These numerous conductance states indicate promising prospects for the application of quantum conductance in polymer-based atomic switches for multilevel data storage.

In addition, Zhu *et al.*[112] documented the conductance quantization observed in various oxide-based devices, including Nb/ZnO/Pt and ITO/ZnO/ITO systems. They demonstrated the ability to effectively modulate conductance quantization

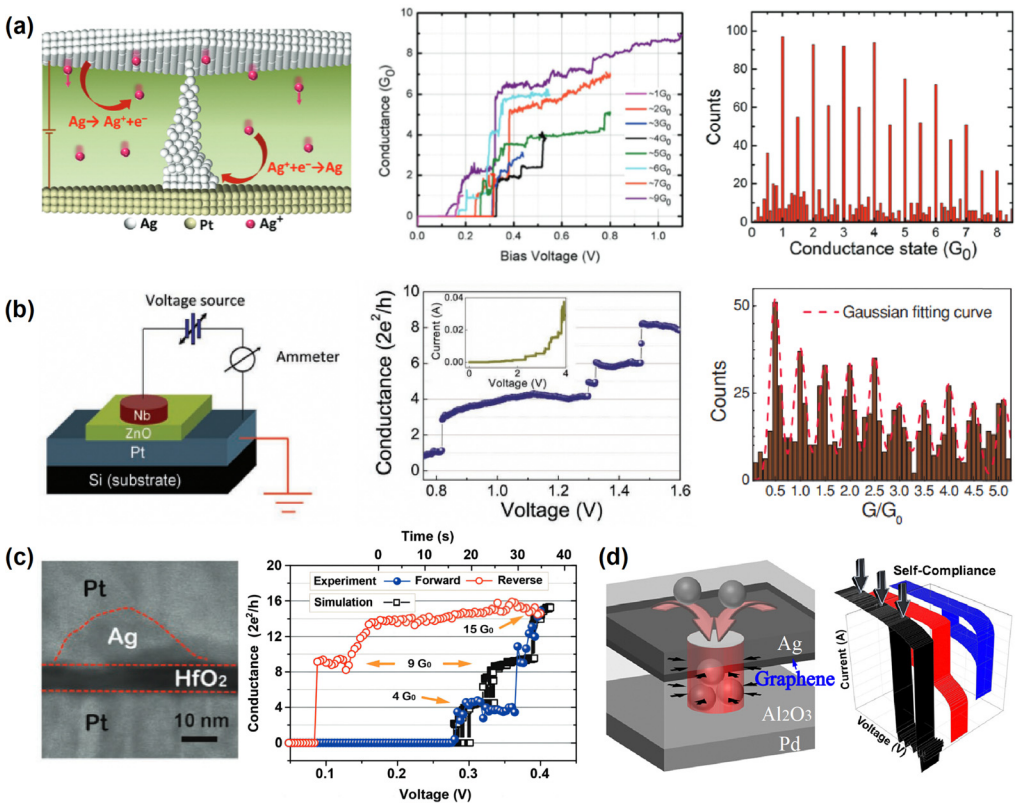

Fig. 11 Quantum conductance for memory applications. (a) Schematic of the APC structures in the Ag/PEO/Pt device under forward bias (left). Multilevel quantum conductance states in the Ag/PEO/Pt device (middle). Conductance state histograms in G_0 evaluated from 360 sweep cycles (right).[116] (b) Schematic of a sandwiched Nb/ZnO/Pt structure (left). The quantum conductance step occurs during the set process in the Nb/ZnO/Pt device (middle). Histogram of conductance values of ITO/ZnO/ITO devices (right).[112] (c) HAADF-STEM cross-sectional image of AND-TS stack layers and conductance quantization characteristics of the AND-TS device.[117] (d) Schematic of the Ag/graphene/Al_2O_3-based TS device with self-compliance.[118]

behaviors in these systems. The current jumps were initially observed during the set process of Nb/ZnO/Pt sandwich structures, corresponding to abrupt changes in conductance. Following each change, a stable platform was detected as shown in Fig. 11b. They suggested that this distinctive quantized conductance behavior is a common characteristic of RRAM devices founded on conductive filaments. Consequently, the study of quantized conductance behavior was extended to the ITO/ZnO/ITO device, which exhibited unipolar RS behaviors instead of bipolar switching observed in the Nb/ZnO/Pt device. The statistical histogram of conductance revealed that the values were concentrated near half-integer multiples of G_0, similar to the bipolar resistance switching characteristics seen in the Nb/ZnO/Pt devices. These findings demonstrate that controllable atomic-scale conduction channels can be constructed in simple two-terminal devices in air and at room temperature, providing a platform for the development of new nano-devices based on quantum effects.

Selectors play a crucial role in mitigating leakage interference among storage cells within cross-point arrays, requiring high selectivity and minimal leakage currents to reduce sneak currents and power consumption. However, conventional selectors typically exhibit limited on-state currents ($\leq$10 μA), which are inadequate for memory reset operations. Selector configurations like one-transistor-one-resistor (1T1R) compromise the scaling advantages of crosspoint architectures due to the large feature size of the transistor. In contrast, the one-selector-one-resistor (1S1R) configuration is better suited for *x*-point integration but suffers from high leakage current issues. Hua *et al.*[117] addressed these challenges by developing Ag nanodots/HfO_2-based selectors, where they directly observed significant jumps in quantized conductance at 4, 9, and 15 G_0 by employing rapidly heat-treated Ag nanodots (Fig. 11c). Through exploiting the spontaneous rupture of delicate Ag filaments at the APC level with decreasing applied voltage, a selector could be achieved with a RESET current of approximately 2.3 mA, bidirectional threshold switching, no need for electrostatic formation, and exceptional selectivity exceeding 10^9. It also displayed ultra-low leakage current below 1 pA, a remarkably steep slope of 0.65 mV dec^{-1}, and robust thermal stability up to 200 °C. Furthermore, this selector demonstrated notable rejection of leakage current and exceptional SET/RESET operation performance within a 1S1R configuration.

In another study, Song *et al.*[118] introduced a technique involving the insertion of an engineered defective graphene monolayer between the Ag electrode and the Al_2O_3 electrolyte (Fig. 11d). This method effectively restricted Ag ion migration and controlled the size and density of Ag filaments, facilitating contact with Ag ions solely for the formation of an APC structure. Experimentally, they observed significant quantized conductance jumps from 11 to 21 G_0. Capitalizing on these merits, they fabricated Ag/graphene/Al-based selectors with exceptional selectivity and adaptability, reaching levels on the order of 10^{10}. These selectors exhibited an extremely low turn-off current of 0.1 pA and demonstrated switching slopes of 1.13 mV dec^{-1} and 1.11 mV dec^{-1} for on and off states, respectively. This work proved the significance of constructing an APC structure in the preparation of selectors with outstanding performance and minimal leakage current.

5.2. Computing

Except for multilevel data storage, quantum conductance within APC structures also holds promise for logic circuits. As leading candidates for advanced computing applications, memristors are being developed as key components in transient electronics. To date, the modulation of quantum conductance has been observed in memristors incorporating various metal oxides.[119] Moreover, similar controllability has been demonstrated in transient materials. Zhao *et al.*[120] presented a self-supporting lightweight memristor constructed from acidic polysaccharides as displayed in Fig. 12a. Due to the ability of Mg cations to interact with ionized acid groups, acidic polysaccharides can effectively confine ions. By utilizing these polysaccharides as the resistance-switching layer, enhanced precision in controlling conductive pathways can be achieved. In the Mg/pectin/Mg sandwich structure, 16 continuous quantum conductance states were achieved, measured in units of G_0 (Fig. 12b). Remarkably, this quantum conductance switch presented an ultra-fast operational speed (2–5 ns) and low energy consumption (0.6–16 pJ). These properties positioned it as a promising candidate for incorporation into fast, low-power, high-density memory designs. Furthermore, the effective control of multiple quantum conductance states within a single device represented a significant advancement toward achieving quantized multi-bit storage and computing functionalities. Encoding stands as the primary mechanism of storage, facilitating the conversion of diverse forms of information such as words, images, and sounds into a storable format. This enables their recording, subsequent extraction, and utilization in subsequent storage stages. Zhao *et al.* further labeled the 16 quantum conductance states within a single Mg/pectin/Mg memristor as 16 distinct codes, with each code corresponding to a four-bit binary number. By employing two memristor units, they successfully encoded the sequence ''NENU'', thereby conserving storage space (Fig. 12c).

Terabe *et al.*[15] demonstrated that all requirements for a logic circuit, switching speeds exceeding gigahertz and operational voltages below 1 V, can be met through the utilization of the APC devices. They engineered a vacuum atomic switch using an Ag_2S electrode and a Pt electrode, with an electrode spacing of 1 nm. Upon applying a forward bias to the Ag_2S electrode, an Ag atomic bridge was formed between the two electrodes, inducing the device into a high-conductive state. Conversely, when a negative bias was applied to the Ag_2S electrode, the Ag bridge disintegrated, resetting the device to a low conductive state. This atomic switch was then used to transition between two conductance states, enabling the realization of AND, OR, and NOT gates and facilitating the implementation of all fundamental logic operations as depicted in Fig. 12d. Moreover, the quantum conductance of the 1 × 2 atomic switching array was manipulated through the pulsed bias voltages, allowing for transitions between quantum conductance states. Each

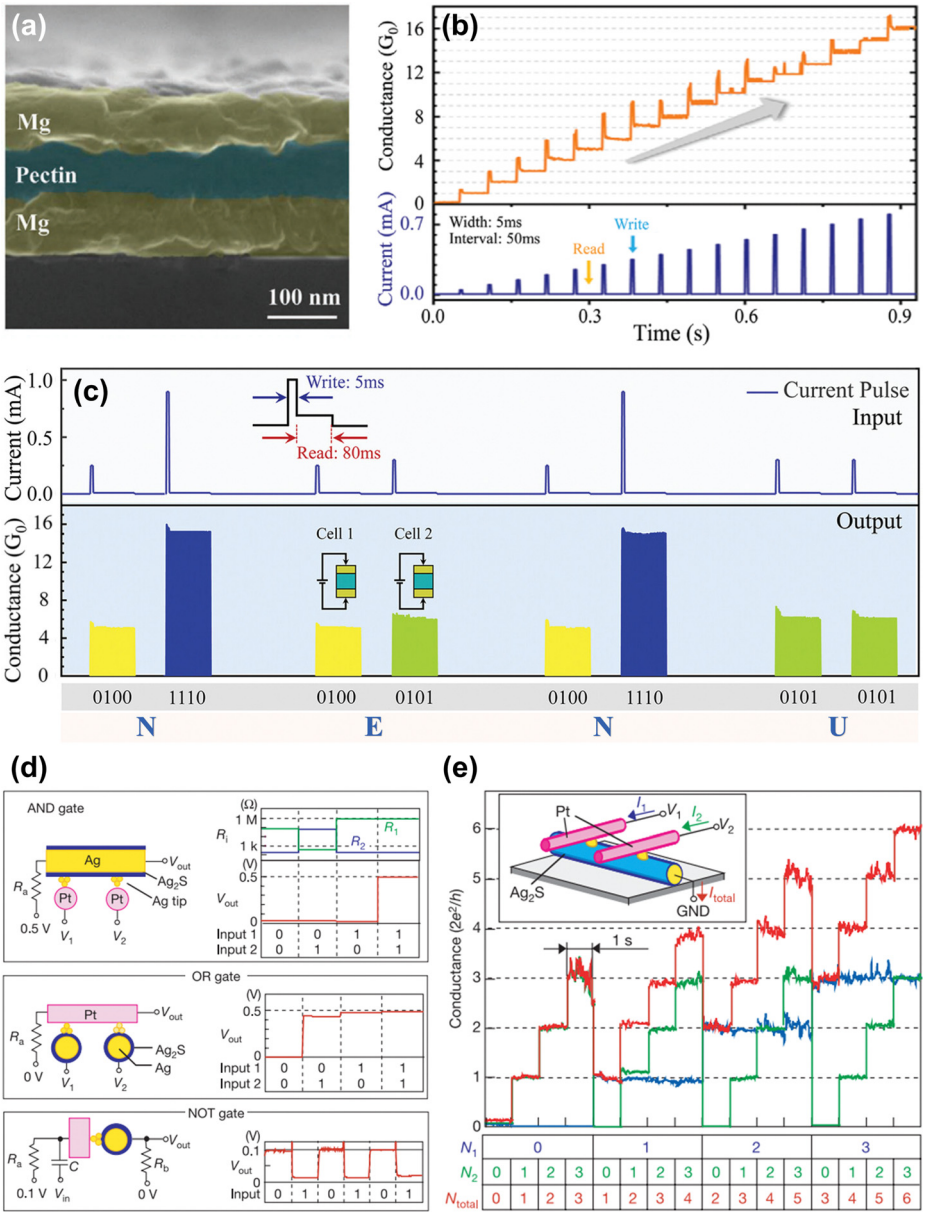

Fig. 12 Quantum conductance for computing applications. (a) Cross-sectional SEM image of the Mg/pectin/Mg device. (b) 16 quantum conductance states were obtained by applying current pulses of different amplitudes. (c) Logic encoding of the word "NENU" according to ASCII.[120] (d) Logic gates configured with the quantum conductance atomic switch (QCAS) made using Ag_2S and Pt electrodes. (e) The conductance of each channel in a 1 × 2 array of QCASs was changed independently from 0 to 3 G_0.[15]

channel's conductance could be independently adjusted from 0 to 3 G_0, enabling the system to function as an adder circuit and serve as a multilevel data memory capable of storing 16 states using only two switches (Fig. 12e).

The synapse serves as the functional connection point between neurons, playing a key role in information transmission. When a presynaptic action potential reaches the synaptic terminal, the voltage-gated calcium (Ca^{2+}) channels are activated, promoting the influx of Ca^{2+} ions through the presynaptic membrane.[121] This triggers changes in synaptic conductivity, resulting in the modulation of excitatory or inhibitory postsynaptic currents (EPSC/IPSC), a key mechanism in the propagation of information within the human neural network. Inspired by this biological process, developing synaptic devices that mimic these functions is essential for advancing artificial neural networks (ANNs), offering a promising alternative to conventional computing architectures.[122] Ion-migration memristors, a common class of synaptic devices, predominantly rely on external electrical stimuli to induce the migration of metal ions or oxygen (or halogen) vacancies, leading to the formation of conductive filaments and atomic point contact (APC) structures.[123] Reverse electrical pulses can drive the migration of these ions or vacancies in the opposite direction, disrupting the filament and modulating changes in electrical conductivity, closely mimicking the behavior of biological synapses. In their work, Ohno *et al.*[124] proposed an Ag_2S inorganic synapse device

that exhibited a transient increase in conductance followed by a spontaneous decay to below 1 G_0 when subjected to input stimuli at a lower repetition rate. Conversely, sustained conductance enhancement beyond 1 G_0 is achieved with frequent input repetition. These findings suggest that individual inorganic synapse elements could serve as innovative functional components for neural systems that are capable of operating independently of software and pre-programming, unlike current artificial neural network systems. Meanwhile, they constructed a psychological model related to memory and forgetting processes, noting that the decay of conductance in the short-term memory (STM) mode mirrored the 'forgetting curve'.

Compared to memristors based on metal oxides and chalcogenides, organic polymer-based electrochemical metallization (ECM) systems offer a promising avenue for precise control of conductive filaments at the atomic scale, enabling multilevel quantum conductance behavior under ambient conditions.[125] Krishnan *et al.* reported an essential ion-conducting insulating layer using a polyvinyl imidazole (PVI) polymer for an Ag-PVI ECM-based memristor (Fig. 13a-c).[60] The device exhibited stable resistive switching and highly controllable transitions from single to multi-level quantum conductance states with increasing stop voltage. The conductance stability exhibited an exponential increase, with a maximum retention time of approximately 50 minutes achieved for $\sim$10 G_0 at room temperature. Moreover, the fabricated memristors successfully emulated diverse synaptic functions, including learning and forgetting behaviors. Simultaneous current–voltage and cyclic voltammetry studies revealed that the confined atomic redox process occurred within the narrowest region of the conducting channel in the Ag-PVI memristor. This study underscores the importance of quantum conductance in advancing the understanding and implementation of artificial synapses.

A neuromorphic computing system emulates the neurons and synapses found in the human brain.[127] It is adept at handling complex and unstructured information, enabling learning and memory processes through parallel chemical interactions. Recently, Lee *et al.*[128] introduced a Pt/Al_2O_3/TaN device as a candidate for the neuromorphic device. During retention tests, the reset process consistently revealed a gradual decrease in current, supporting the existence of diverse multi-level states. The phenomenon of conductance quantization was further validated. The phenomenon of conductance quantization was confirmed, with the histogram plot showing a pronounced clustering around multiples or half-multiples of G_0 across various conductance steps. Meanwhile, the values displayed discernible distinctions between 0.5 and 3 G_0. To enhance the resolution and distinguishability of quantized values, it may be imperative to reduce the size of the conducting filament through techniques such as scaling down the device dimensions. The neuromorphic computing system was further developed using multi-level cells in Pt/Al_2O_3/TaN devices, where pulse measurements demonstrated continuous modulation of conductance through five cycles of potentiation and depression pulses. The *I–V* characteristic analysis during the set process showed an abrupt potentiation, while the depression phase followed a more gradual profile. By adjusting the pulse voltage amplitude, more gradual and symmetric conductance-change characteristics were achieved. Additionally, simulation results of MNIST pattern recognition utilizing this conductance data were presented, confirming that the conductance quantization phenomenon, observed during the reset process and pulse measurements, facilitated a more efficient learning process.

Jeon *et al.*[126] proposed a unique Ta_2O_5/HfO_2 double-layer structure, which effectively controls Ag ion diffusion due to the different oxidation ratios between the layers, as shown in Fig. 13d–f. The presence of distinct oxygen vacancy layers allowed precise control over the conductive filament, generating multi-level volatile switching and demonstrating the quantum conductance effect controlled by Ag atoms. During pulse measurements, the current levels decayed discretely, reflecting dynamics of the device's conductance over time. With repeated stimulation, the quantum conductance decreased from four to three steps, eventually transitioning to behavior consistent with classical physics. This shift highlights the device's ability to transition from short-term to long-term plasticity, a key feature of synaptic behavior. The double-layer device achieved an operating voltage of 0.2 V, an on/off ratio of 10^9, and a power consumption of 2 mW, outperforming previously reported devices that utilized metal-based oxides. These results highlight the significance of controlling Ag migration at the bilayer interface to enhance the synaptic properties and overall performance of neuromorphic devices.

5.3. Encryption

Nowadays, the advancement of the Internet of Things (IoT) necessitates the development of cost-effective, compact, lightweight, and dependable true random number generator (TRNG) circuits for encrypting data generated by objects or humans before transmission. State-of-the-art TRNG circuits typically utilize an entropy source to produce sequences of unpredictable binary numbers, exploiting phenomena such as the thermal noise of resistors, the jitter of ring oscillators, and the metastability of flip-flops (as shown in Fig. 14a).[24] However, these circuits often suffer from high power consumption and limited scalability and are frequently confined to the simulation stage. Quantum conductance is driven by quantum mechanical effects, such as electron wave behavior and tunneling, which introduce uncertainty at the microscopic scale. This makes it possible to generate high-quality random number sequences by measuring conductance. Therefore, random number generators can harness the physical mechanisms of quantum conductance to provide a reliable source of randomness for information security and computing. Meanwhile, due to the polymorphic nature of the quantum conductance effect, it could be an efficient entropy source for TRNG circuits because they can produce random variations of different magnitudes during operation while consuming little energy.

Nanoionic memristors with tunable conductance, capable of achieving multiple levels through the application of electrical

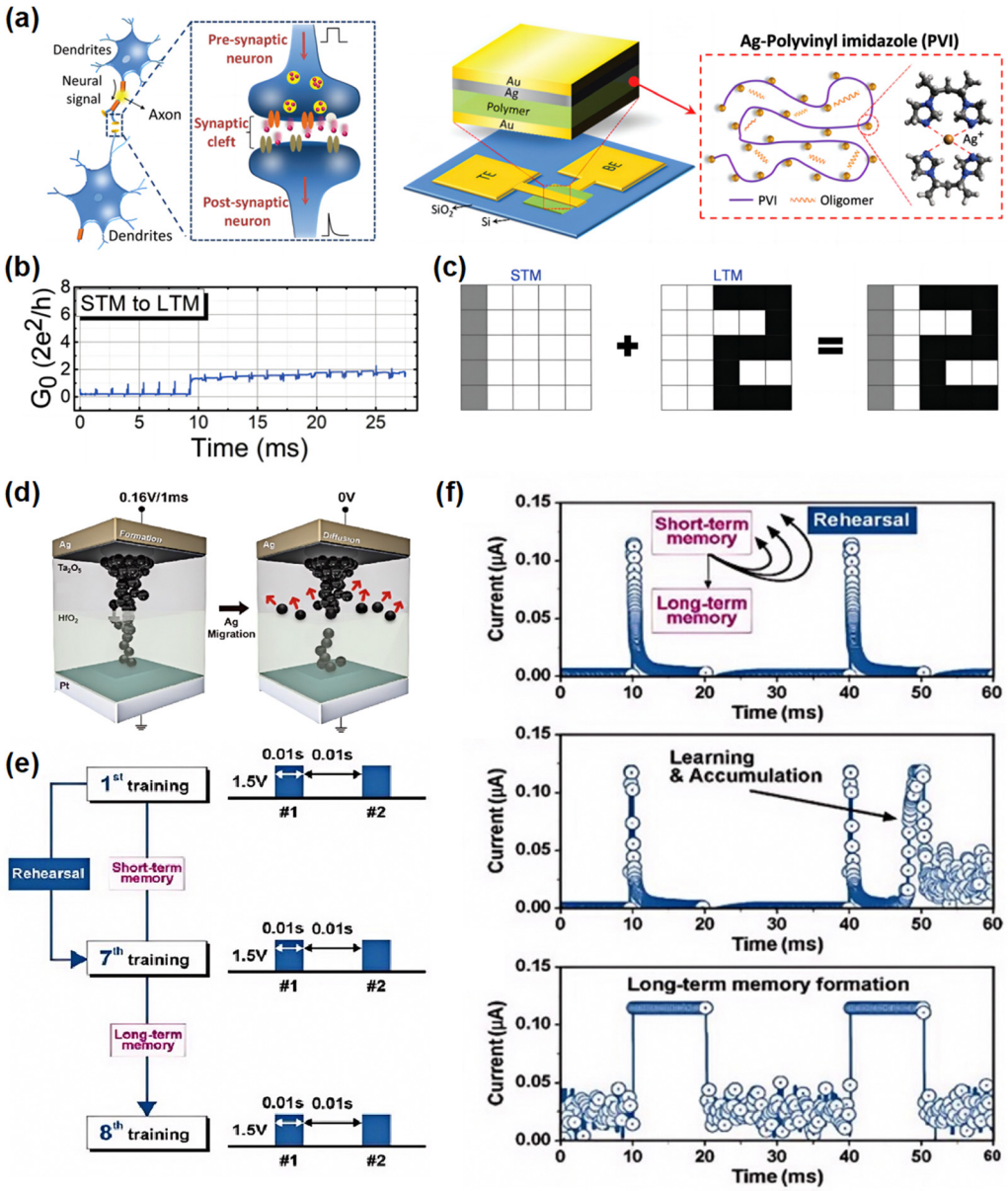

Fig. 13 Quantum conductance for neuromorphic computing applications. (a) Schematic of the biological synapse illustrating the synaptic behavior between the pre-synaptic and post-synaptic neurons (left panel). Schematic of the Ag/Ag-PVI/Au device (right panel). (b) The transition from STM to LTM transition. (c) Schematic representation of memorizing the numerical letters "1" (STM) and "2" (LTM).[60] (d) Schematic representation of the Ta_2O_5/HfO_2 double-layer structure before and after Ag migration. The metal filament was formed by the 0.16 V/1 ms pulse but metal ions diffused after the pulse. (e) and (f) The transition from STM to LTM through the rehearsal with the repetitive training pulse of a pair 1.5 V/0.01 s. The right panel shows the initial state of the device and after the 7th and 8th training, respectively.[126]

stress sequences, represent a promising alternative.[131,132] Song *et al.*[133] developed a TiO_x/Al_2O_3 memristor that utilizes random telegraph noise (RTN) as an entropy source. In this oxide-based memristor, charge transport is primarily controlled by trap-assisted tunneling at oxygen vacancies. The RTN signals are predominantly influenced by the current contribution of a single-dominant oxygen vacancy, resulting in two-level RTN signals. These RTN-induced current fluctuations are more observable at the low-conductance state (LCS), where device conduction is limited by the tunneling gap, corresponding to a quantized conductance value of about 2.5 G_0. In contrast, at the high-conductance state (HCS), RTN signals are less pronounced due to the current flowing through a conductive filament in the switching layer, resulting in a lower conductance of 0.4 G_0. Experimental results demonstrate that among the 60 000 bits generated by the TRNG circuit, the percentages of 0 and 1 are 49.97% and 50.03%, respectively, indicating unbiased random bit generation. Furthermore, the TRNG remains functional in the digital mode even with multilevel RTN signals, as long as a dominant trap significantly influences device conduction

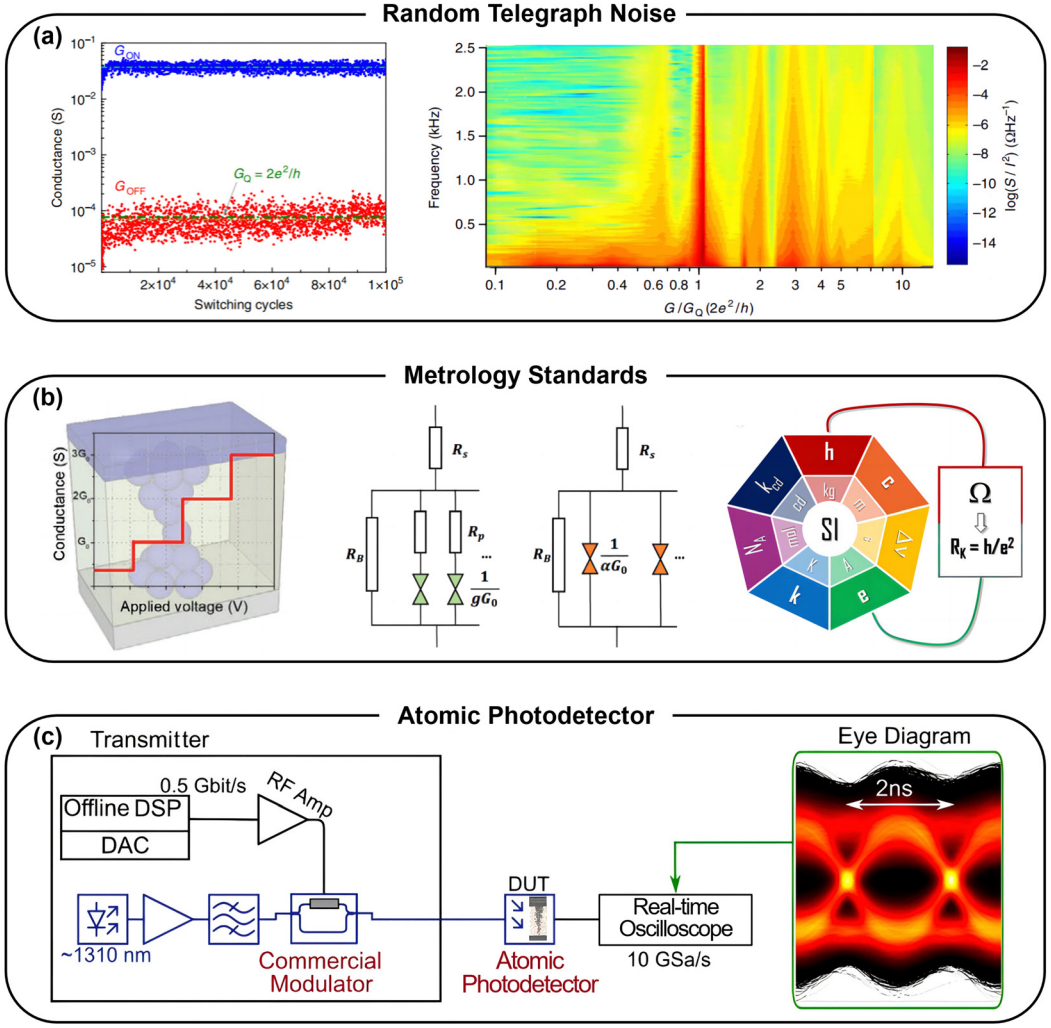

Fig. 14 Quantum conductance for random telegraph noise, metrology standards, and atomic photodetector applications. (a) Images showing "Random Telegraph Noise": conductance switching data of a TaO_x memristor for 100 000 switching cycles showing larger variance in the regime close to a quantum of conductance, and a two-dimensional color plot showing S/I^2 as a function of conductance G/G_Q and frequency f at T = 295 K. The continuous scale on the color plot was obtained by linear interpolation between measured data points. This representation reveals the markedly increased noise near the first conductance quantum G_Q and the tails of the noise distribution as a function of frequency.[24] (b) Images showing "Metrology Standards": the schematization of quantum steps in memristive devices,[34] the equivalent electrical circuit of a memristive device,[129] units and defining constants in the revised SI.[130] (c) Images showing an "Atomic Photodetector": a random bit-pattern at 0.5 Gbit s^{-1} was generated with an offline DSP and encoded by means of a commercial modulator onto a laser signal. The signal was then detected using the atomic scale photodetector.[71]

compared to other traps. The generated random number dataset passed all 16 NIST tests, confirming its robustness and compliance with established randomness standards.

In addition, the 2D multi-layer h-BN was employed as an insulating layer to fabricate an Ag/h-BN/Ag memristor film by Pazos *et al.*,[134] which exhibited exceptional RTN current signals. This h-BN-based memristor demonstrated low-power operation (approximately 650 nW) and retained highly stable RTN current signals for extended durations (exceeding 1 hour), marking one of the longest durations reported to date. Given their inherent time-domain randomness, the RTN signals generated by Ag/h-BN/Ag memristors hold promise for utilization in TRNG circuits, facilitating advanced data encryption and the generation of one-time authentication factors. Moreover, interfacing h-BN memristors with a commercial microcontroller led to the creation of a highly reliable and low-power standalone hardware solution for TRNG generation. This system exhibited robustness not only against temporary interruptions of the RTN signal but also against fluctuations in the characteristics of the entropy source.

5.4. Others

When the size of a conductor approaches the atomic scale, electrons undergo ballistic transport without scattering from each other, leading to the manifestation of quantum conductance effects. As the conductance quantum ($G_0 = 2e^2/h$) is determined solely by the fundamental constants of nature, it serves as a resistance standard, thus contributing to the

revision of the International System of Units (SI) in 2019 (as shown in Fig. 14b).[130] Unlike standard resistors, which are typically derived from the quantum Hall effect, those based on the quantum conductance effect can operate at room temperature, in ambient air, and without requiring a magnetic field, making them suitable for chip integration. Jordi Suñé *et al.*[129] constructed a device consisting of $Al_2O_3/HfO_2/Al_2O_3/HfO_2/Al_2O_3$ nanolaminate insulators and Al as the top and bottom electrodes, respectively. This design uses the irreversibility of breakdown filaments, enhancing stability and facilitating statistical analysis of quantum conductance phenomena. The commercial resistors could achieve accuracies of up to 0.01%, while the uncertainty associated with the quantum Hall resistor standard was approximately 10^{-9}. Despite these impressive standards, the sample-to-sample variation of around 15% when using quantum conductance was too large for this application. Although current results did not meet the required accuracy, optimizing insulator design and electrical stressing techniques could improve control over filament shape, potentially reducing sample-to-sample variations to levels suitable for resistive standard applications. These advancements are essential for integrating fundamental units on-chip and realizing self-calibrating systems with zero-chain traceability. Meanwhile, Delfanazari *et al.* achieved the first experimental observation of conductance quantization in a hybrid InGaAs–Nb APC structure.[135] Repeatable quantized conductance was observed at zero magnetic fields across multiple quantum nanodevices fabricated on a single chip. These intrinsic properties make them invaluable for quantum metrology, particularly for establishing extremely precise and stable voltage standards.

The inherent limitation of CMOS scaling can be addressed by using optical manipulation of atomic rearrangements within metal quantum dot contacts. This approach facilitates the development of optically controlled electronic switches by creating a platform that integrates electronics and photonics at the atomic scale (as shown in Fig. 14c). Recently, a pyramid-like 3D plasmonic tip composed of Ag-α-SiO_2-Pt was fabricated by Emboras *et al.*[71] By applying a bias voltage to the metal tip, they induced the formation of an atomic-scale filament that created a short circuit between the two metals. Subsequently, directing light onto a small area of the plasmonic tip caused reversible atomic movements between adjacent positions under illumination. These atomic rearrangements corresponded to transitions between different electronic quantum states. Despite its small size, the device exhibited impressive characteristics, including a notable resistive extinction ratio of 70 dB, a low shutdown current in the range of tens of picoamps, and reliable operation over weeks at room temperature. It delivered a characteristic hysteresis loop typical of a memristor driven by light rather than electricity, maintaining reliable performance over millions of operational cycles. Therefore, integrating the atomic point contact (APC) structure with electronics and photonics is promising for the development of innovative optoelectronic platforms, with potential applications such as digital photodetectors that bypass the need for decision-making circuits or analog-to-digital converters.

6. Summary and outlook

The development of reconfigurable atomic precision control (APC) structures through nanoionics technology offers a promising avenue for achieving atomic-level precision alongside quantum conductance effects. Several excellent review articles have thoroughly examined the advancements in these devices. Recent research underscores the growing interest in exploring one-dimensional (1D) and two-dimensional (2D) materials beyond the conventional oxide materials typically used for APC structure development. Additionally, studies on the influence of various external fields—including electric, optical, magnetic fields and mechanical stresses—on quantum effects within APC structures reveal their significant impact on quantum conductance. This review paper explores these aspects, aiming to deepen our understanding of the complex relationship between quantum conductance phenomena, materials' properties, and external fields, thereby contributing valuable insights into these rapidly evolving areas of research.

So far, the resistance-switching devices (known as the memristors) have been considered promising for constructing APC structures and achieving quantum conductance. These devices generate conductive filament channels at the atomic level through ion migration within the dielectric layer, offering an efficient method for precise quantum conductance regulation. Over the past few decades, significant progress has been made in both the theoretical understanding and experimental observation of quantum conductance in APC structures within memristors. Memristors embedded with APC are valued for their ability to retain historical electrical signal information, ultra-low power consumption, ultra-fast response speeds, and precisely adjustable multi-level quantum conductance states. They are considered highly suitable for applications such as high-density storage, memory logic circuits, synaptic simulation, photon detection, and neuromorphic computing. They offer a promising strategy for managing the massive data growth of the information age.

However, the practical application of quantum conductance effects in APC structures still faces several challenges. The origin of stepwise variations in quantum conductance requires additional investigation to clarify the relationship between this phenomenon and discrete atomic structures. Moreover, improving the controllability and stability of quantum conductance states involves understanding the interaction between medium materials and migrating ions to achieve rational coupling of APC components and storage media. To precisely control and adjust quantum conductance levels, further exploration of the relationships between migrating ions, medium materials, operating parameters, and device functionalities is needed, which will guide future optimization of memristor performance. Additionally, it is crucial to pay close attention to other physical properties associated with quantum conductance states, including thermoelectricity, photovoltaics, superconductivity, and magnetoresistance effects. To enhance the reliability of device operation, it is imperative to develop advanced methods aimed at improving material quality and

addressing defect characteristics in design. Besides, refining processing technology to achieve high crystallinity and uniform thickness of materials will help minimize sample variations. Future challenges include wafer-level device manufacturing, high-density integration, and multifunctional interconnection. Addressing these challenges will be crucial for the practical application of quantum conductance technology. Given its numerous characteristics and advantages, quantum conductance holds great promise for the information field, and ongoing exploration is expected to lead to rapid development and a wide range of applications in the near future.

Data availability

The data that support the findings of this study are available upon reasonable request.

Conflicts of interest

There are no conflicts to declare.

Acknowledgements

This work was supported by the Natural Science Foundation of Zhejiang Province (LDQ23E020001), National Natural Science Foundation of China (62174164, U23A20568, and U22A2075), National Key Research and Development Project (2021YFA1202600), China Postdoctoral Science Foundation (2023M743630), Talent Plan of Shanghai Branch, Chinese Academy of Sciences (CASSHB-QNPD-2023-022), Ningbo Technology Project (2022A-007-C), and Ningbo Key Research and Development Project (2023Z021).

References

1 A. Biswas and H.-C. Wang, *Sensors*, 2023, **23**, 1963.
2 H. Hua, Y. Li, T. Wang, N. Dong, W. Li and J. Cao, *ACM Comput. Surv.*, 2023, **55**, 1–35.
3 G.-S. Jeong, W. Bae and D.-K. Jeong, *Sensors*, 2017, **17**, 1962.
4 F. Fang, N. Zhang, D. Guo, K. Ehmann, B. Cheung, K. Liu and K. Yamamura, *Int. J. Extreme Manuf.*, 2019, **1**, 012001.
5 Y. Yang, C. Gu and J. Li, *Small*, 2019, **15**, 1804177.
6 J. Wang, F. Sciarrino, A. Laing and M. G. Thompson, *Nat. Photonics*, 2020, **14**, 273–284.
7 M. Krelina, *EPJ Quantum Technol.*, 2021, **8**, 24.
8 A. J. Heinrich, W. D. Oliver, L. M. Vandersypen, A. Ardavan, R. Sessoli, D. Loss, A. B. Jayich, J. Fernandez-Rossier, A. Laucht and A. Morello, *Nat. Nanotechnol.*, 2021, **16**, 1318–1329.
9 T. Proctor, K. Rudinger, K. Young, E. Nielsen and R. Blume-Kohout, *Nat. Phys.*, 2022, **18**, 75–79.
10 F. Xie, A. Peukert, T. Bender, C. Obermair, F. Wertz, P. Schmieder and T. Schimmel, *Adv. Mater.*, 2018, **30**, 1801225.
11 A. Wedig, M. Luebben, D.-Y. Cho, M. Moors, K. Skaja, V. Rana, T. Hasegawa, K. K. Adepalli, B. Yildiz and R. Waser, *Nat. Nanotechnol.*, 2016, **11**, 67–74.
12 J. Gooth, M. Borg, H. Schmid, V. Schaller, S. Wirths, K. Moselund, M. Luisier, S. Karg and H. Riel, *Nano Lett.*, 2017, **17**, 2596–2602.
13 W. Zhang, H. Liu, J. Lu, L. Ni, H. Liu, Q. Li, M. Qiu, B. Xu, T. Lee and Z. Zhao, *Light: Sci. Appl.*, 2019, **8**, 34.
14 N. Tombros, A. Veligura, J. Junesch, M. H. D. Guimarães, I. J. Vera-Marun, H. T. Jonkman and B. J. van Wees, *Nat. Phys.*, 2011, **7**, 697–700.
15 K. Terabe, T. Hasegawa, T. Nakayama and M. Aono, *Nature*, 2005, **433**, 47–50.
16 S. Caneva, P. Gehring, V. M. García-Suárez, A. García-Fuente, D. Stefani, I. J. Olavarria-Contreras, J. Ferrer, C. Dekker and H. S. J. van der Zant, *Nat. Nanotechnol.*, 2018, **13**, 1126–1131.
17 C. Borja, C. Sabater, C. Untiedt, E. Medina and W. Brämer-Escamilla, *Eur. J. Phys.*, 2020, **41**, 065401.
18 K. Terabe, T. Tsuchiya, R. Yang and M. Aono, *Nanoscale*, 2016, **8**, 13873–13879.
19 J. Zhang, W. Liu, J. Dai and K. Xiao, *Adv. Sci.*, 2022, **9**, 2200534.
20 R. Gao, J. Tang, K. Zhang, K. Ozawa and L.-C. Qin, *Nano Energy*, 2020, **78**, 105341.
21 M. Parrilla, M. Cuartero and G. A. Crespo, *Trends Anal. Chem.*, 2019, **110**, 303–320.
22 Y. Yang and R. Huang, *Nat. Electron.*, 2018, **1**, 274–287.
23 T. Takahashi and O. Yamamoto, *J. Appl. Electrochem.*, 1973, **3**, 129–135.
24 W. Yi, S. E. Savel'ev, G. Medeiros-Ribeiro, F. Miao, M. X. Zhang, J. J. Yang, A. M. Bratkovsky and R. S. Williams, *Nat. Commun.*, 2016, **7**, 11142.
25 M. Ismail, C. Mahata, M. Kang and S. Kim, *Nanoscale Res. Lett.*, 2022, **17**, 61.
26 O. G. Kharlanov, B. S. Shvetsov, V. V. Rylkov and A. A. Minnekhanov, *Phys. Rev. Appl.*, 2022, **17**, 054035.
27 C. Z. Li and N. J. Tao, *Appl. Phys. Lett.*, 1998, **72**, 894–896.
28 S. Seo, *et al.*, *Appl. Phys. Lett.*, 2004, **85**, 5655–5657.
29 S. Seo, *et al.*, *Appl. Phys. Lett.*, 2005, **86**, 093509.
30 K. Terabe, T. Hasegawa, T. Nakayama and M. Aono, *Riken Rev.*, 2001, 7–8.
31 L. Olesen, E. Lægsgaard, I. Stensgaard, F. Besenbacher, J. Schio, P. Stoltze, K. W. Jacobsen and J. No, *Phys. Rev. Lett.*, 1994, **72**, 2251.
32 J. L. Costa-Krämer, N. García, P. García-Mochales, P. A. Serena, M. I. Marqués and A. Correia, *Phys. Rev. B: Condens. Matter Mater. Phys.*, 1997, **55**, 5416–5424.
33 K. Terabe, T. Tsuchiya and T. Tsuruoka, *Adv. Phys.: X*, 2022, **7**, 2065217.
34 G. Milano, M. Aono, L. Boarino, U. Celano, T. Hasegawa, M. Kozicki, S. Majumdar, M. Menghini, E. Miranda and C. Ricciardi, *Adv. Mater.*, 2022, **34**, 2201248.
35 C. Mahata, M. Ismail and S. Kim, *Appl. Phys. Lett.*, 2021, **119**, 221601.

36 Z. Xie, S. Gao, X. Ye, H. Yang, G. Gong, Y. Lu, J. Ye, G. Liu and R.-W. Li, *Phys. Chem. Chem. Phys.*, 2020, **22**, 26322–26329.
37 R. Waser and M. Aono, *Nat. Mater.*, 2007, **6**, 833–840.
38 M.-J. Lee, *et al.*, *Nat. Mater.*, 2011, **10**, 625–630.
39 C. A. Polanco, A. van Roekeghem, B. Brisuda, L. Saminadayar, O. Bourgeois and N. Mingo, *Sci. Adv.*, 2023, **9**, eadi7439.
40 B. J. van Wees, H. van Houten, C. W. J. Beenakker, J. G. Williamson, L. P. Kouwenhoven, D. van der Marel and C. T. Foxon, *Phys. Rev. Lett.*, 1988, **60**, 848–850.
41 H. Ohnishi, Y. Kondo and K. Takayanagi, *Nature*, 1998, **395**, 780–783.
42 N. Goel, J. Graham, J. C. Keay, K. Suzuki, S. Miyashita, M. B. Santos and Y. Hirayama, *Phys. E*, 2005, **26**, 455–459.
43 U. M. Kannan, S. Kuntz, O. Berg, W. Kittler, H. Basumatary, J. Arout Chelvane, C. Sürgers and S. Narayana Jammalamadaka, *Appl. Phys. Lett.*, 2016, **108**, 242408.
44 S. Egle, C. Bacca, H.-F. Pernau, M. Huefner, D. Hinzke, U. Nowak and E. Scheer, *Phys. Rev. B: Condens. Matter Mater. Phys.*, 2010, **81**, 134402.
45 J. M. Krans, J. M. van Ruitenbeek, V. V. Fisun, I. K. Yanson and L. J. de Jongh, *Nature*, 1995, **375**, 767–769.
46 A. Halbritter, P. Makk, S. Mackowiak, S. Csonka, M. Wawrzyniak and J. Martinek, *Phys. Rev. Lett.*, 2010, **105**, 266805.
47 T. Nakazumi, Y. Wada and M. Kiguchi, *Nanotechnology*, 2012, **23**, 405702.
48 C. J. Muller, J. M. Krans, T. N. Todorov and M. A. Reed, *Phys. Rev. B: Condens. Matter Mater. Phys.*, 1996, **53**, 1022–1025.
49 F. Strigl, C. Espy, M. Bückle, E. Scheer and T. Pietsch, *Nat. Commun.*, 2015, **6**, 6172.
50 D.-M. Tang, L.-C. Yin, F. Li, C. Liu, W.-J. Yu, P.-X. Hou, B. Wu, Y.-H. Lee, X.-L. Ma and H.-M. Cheng, *Proc. Natl. Acad. Sci. U. S. A.*, 2010, **107**, 9055–9059.
51 D. M. Eigler and E. K. Schweizer, *Nature*, 1990, **344**, 524–526.
52 H. D. Chopra, M. R. Sullivan, J. N. Armstrong and S. Z. Hua, *Nat. Mater.*, 2005, **4**, 832–837.
53 A. Sokolov, C. Zhang, E. Y. Tsymbal, J. Redepenning and B. Doudin, *Nat. Nanotechnol.*, 2007, **2**, 171–175.
54 D. A. Ryndyk, *Theory of Quantum Transport at Nanoscale*, Springer, 2016.
55 T. Ouisse, *Electron Transport in Nanostructures and Mesoscopic Devices: An Introduction*, John Wiley & Sons, 2013.
56 W. Xue, S. Gao, J. Shang, X. Yi, G. Liu and R.-W. Li, *Adv. Electron. Mater.*, 2019, **5**, 1800854.
57 D. Wang, F. Ji, X. Chen, Y. Li, B. Ding and Y. Zhang, *Appl. Phys. Lett.*, 2017, **110**, 093501.
58 L. Jiang, L. Xu, J. W. Chen, P. Yan, K. H. Xue, H. J. Sun and X. S. Miao, *Appl. Phys. Lett.*, 2016, **109**, 153506.
59 J. Zhao, *et al.*, *J. Mater. Chem. C*, 2019, **7**, 1298–1306.
60 K. Krishnan and S. Vijayaraghavan, *Adv. Electron. Mater.*, 2022, **8**, 2200509.
61 S. R. Nandakumar, M. Minvielle, S. Nagar, C. Dubourdieu and B. Rajendran, *Nano Lett.*, 2016, **16**, 1602–1608.
62 Y. Yang, J. Liu, J. Zheng, M. Lu, J. Shi, W. Hong, F. Yang and Z. Tian, *Nano Res.*, 2017, **10**, 3314–3323.
63 F. L. Aguirre, *et al.*, *Sci. Rep.*, 2024, **14**, 1122.
64 C. Mahata, M. Ismail, M. Kang and S. Kim, *Nanoscale Res. Lett.*, 2022, **17**, 58.
65 W. Xue, *et al.*, *Adv. Electron. Mater.*, 2020, **6**, 1901055.
66 M.-H. Peng, C.-Y. Pan, H.-X. Zheng, T.-C. Chang and P.-H. Jiang, *ACS Appl. Nano Mater.*, 2021, **4**, 11296–11304.
67 J. Dong, A. Suwardi, X. Y. Tan, N. Jia, K. Saglik, R. Ji, X. Wang, Q. Zhu, J. Xu and Q. Yan, *Mater. Today*, 2023, **66**, 137–157.
68 S. Kaeriyama, T. Sakamoto, H. Sunamura, M. Mizuno, H. Kawaura, T. Hasegawa, K. Terabe, T. Nakayama and M. Aono, *IEEE J. Solid-State Circuits*, 2005, **40**, 168–176.
69 K. Terabe, T. Hasegawa, C. Liang and M. Aono, *Sci. Technol. Adv. Mater.*, 2007, **8**, 536–542.
70 D. Zheng, *et al.*, *Nanophotonics*, 2021, **10**, 4637–4644.
71 A. Emboras, *et al.*, *ACS Nano*, 2018, **12**, 6706–6713.
72 G. Milano, F. Raffone, K. Bejtka, I. De Carlo, M. Fretto, F. C. Pirri, G. Cicero, C. Ricciardi and I. Valov, *Nanoscale Horiz.*, 2024, **9**, 416–426.
73 S. Kitsios, P. Bousoulas, D. Spithouris, M. Kainourgiaki, M. Tsigkourakos, P. Chatzopoulou, G. P. Dimitrakopulos, P. Komninou and D. Tsoukalas, *ACS Appl. Electron. Mater.*, 2022, **4**, 2869–2878.
74 J. B. Roldán, D. Maldonado, A. Cantudo, Y. Shen, W. Zheng and M. Lanza, *Appl. Phys. Lett.*, 2023, **122**, 203502.
75 E. Miranda, G. Milano and C. Ricciardi, *IEEE Trans. Nanotechnol.*, 2020, **19**, 297–300.
76 E. Miranda, G. Milano and C. Ricciardi, *IEEE Trans. Nanotechnol.*, 2020, **19**, 609–612.
77 Q. Xia and J. J. Yang, *Nat. Mater.*, 2019, **18**, 309–323.
78 X. Wu, R. Ge, P.-A. Chen, H. Chou, Z. Zhang, Y. Zhang, S. Banerjee, M.-H. Chiang, J. C. Lee and D. Akinwande, *Adv. Mater.*, 2019, **31**, 1806790.
79 X. Zhao, Z. Fan, H. Xu, Z. Wang, J. Xu, J. Ma and Y. Liu, *J. Mater. Chem. C*, 2018, **6**, 7195–7200.
80 L. Zhang, T. Gong, H. Wang, Z. Guo and H. Zhang, *Nanoscale*, 2019, **11**, 12413–12435.
81 M. E. Turiansky, A. Alkauskas, L. C. Bassett and C. G. Van de Walle, *Phys. Rev. Lett.*, 2019, **123**, 127401.
82 J. Taylor, H. Guo and J. Wang, *Phys. Rev. B: Condens. Matter Mater. Phys.*, 2001, **63**, 245407.
83 V.-N. Do, *Adv. Nat. Sci.: Nanosci. Nanotechnol.*, 2014, **5**, 033001.
84 N. Papior, N. Lorente, T. Frederiksen, A. García and M. Brandbyge, *Comput. Phys. Commun.*, 2017, **212**, 8–24.
85 J. Ferrer, *et al.*, *New J. Phys.*, 2014, **16**, 093029.
86 J. Enkovaara, *et al.*, *J. Phys.: Condens. Matter*, 2010, **22**, 253202.
87 D. Jacob and J. J. Palacios, *J. Chem. Phys.*, 2011, **134**, 044118.
88 A. Hjorth Larsen, *et al.*, *J. Phys.: Condens. Matter*, 2017, **29**, 273002.
89 S. Smidstrup, *et al.*, *J. Phys.: Condens. Matter*, 2020, **32**, 015901.

90 X.-D. Li, N.-K. Chen, B.-Q. Wang and X.-B. Li, *Appl. Phys. Lett.*, 2022, **121**, 073505.
91 K. Krishnan, M. Muruganathan, T. Tsuruoka, H. Mizuta and M. Aono, *Jpn. J. Appl. Phys.*, 2017, **56**, 06GF02.
92 X. Cartoixà, R. Rurali and J. Suñé, *Phys. Rev. B: Condens. Matter Mater. Phys.*, 2012, **86**, 165445.
93 X. Zhong, I. Rungger, P. Zapol and O. Heinonen, *Phys. Rev. B: Condens. Matter Mater. Phys.*, 2016, **94**, 165160.
94 S. Long, X. Lian, C. Cagli, X. Cartoixà, R. Rurali, E. Miranda, D. Jiménez, L. Perniola, M. Liu and J. Suñé, *Appl. Phys. Lett.*, 2013, **102**, 183505.
95 S. Mitra and S. Mahapatra, *npj 2D Mater. Appl.*, 2024, **8**, 26.
96 N. Onofrio and A. Strachan, *J. Chem. Phys.*, 2015, **143**, 054109.
97 S. M. Hus, R. Ge, P.-A. Chen, L. Liang, G. E. Donnelly, W. Ko, F. Huang, M.-H. Chiang, A.-P. Li and D. Akinwande, *Nat. Nanotechnol.*, 2021, **16**, 58–62.
98 W. Song, *et al.*, *Phys. Rev. B: Condens. Matter Mater. Phys.*, 2023, **108**, 045426.
99 T. Kizuka, *Phys. Rev. B: Condens. Matter Mater. Phys.*, 2008, **77**, 155401.
100 L. Cui, W. Jeong, S. Hur, M. Matt, J. C. Klöckner, F. Pauly, P. Nielaba, J. C. Cuevas, E. Meyhofer and P. Reddy, *Science*, 2017, **355**, 1192–1195.
101 A. Wiener, A. I. Fernández-Domínguez, A. P. Horsfield, J. B. Pendry and S. A. Maier, *Nano Lett.*, 2012, **12**, 3308–3314.
102 K. J. Savage, M. M. Hawkeye, R. Esteban, A. G. Borisov, J. Aizpurua and J. J. Baumberg, *Nature*, 2012, **491**, 574–577.
103 I. Köymen, I. D. Carlo, M. Fretto and G. Milano, *IEEE Trans. Electron Devices*, 2024, **71**, 1872–1878.
104 E. Mikheev, I. T. Rosen, J. Kombe, F. Damanet, M. A. Kastner and D. Goldhaber-Gordon, *Nat. Electron.*, 2023, **6**, 417–424.
105 B. Grocholski, *Science*, 2017, **355**, 1169–1171.
106 S. Jezouin, F. D. Parmentier, A. Anthore, U. Gennser, A. Cavanna, Y. Jin and F. Pierre, *Science*, 2013, **342**, 601–604.
107 O. Chiatti, J. T. Nicholls, Y. Y. Proskuryakov, N. Lumpkin, I. Farrer and D. A. Ritchie, *Phys. Rev. Lett.*, 2006, **97**, 056601.
108 M. Z. Hossain, *Appl. Phys. Lett.*, 2010, **96**, 143118.
109 N. Agraït, J. G. Rodrigo and S. Vieira, *Phys. Rev. B: Condens. Matter Mater. Phys.*, 1993, **47**, 12345–12348.
110 Y. Yang, P. Gao, L. Li, X. Pan, S. Tappertzhofen, S. Choi, R. Waser, I. Valov and W. D. Lu, *Nat. Commun.*, 2014, **5**, 4232.
111 S. Tappertzhofen, I. Valov and R. Waser, *Nanotechnology*, 2012, **23**, 145703.
112 X. Zhu, W. Su, Y. Liu, B. Hu, L. Pan, W. Lu, J. Zhang and R.-W. Li, *Adv. Mater.*, 2012, **24**, 3941–3946.
113 J. Zhao, *et al.*, *Appl. Phys. Rev.*, 2022, **9**, 021419.
114 R. D. Nikam, K. G. Rajput and H. Hwang, *Small*, 2021, **17**, 2006760.
115 T. Pelini, *et al.*, *Phys. Rev. Mater.*, 2019, **3**, 094001.
116 K. Krishnan, M. Muruganathan, T. Tsuruoka, H. Mizuta and M. Aono, *Adv. Funct. Mater.*, 2017, **27**, 1605104.
117 Q. Hua, H. Wu, B. Gao, M. Zhao, Y. Li, X. Li, X. Hou, M.-F. Chang, P. Zhou and H. Qian, *Adv. Sci.*, 2019, **6**, 1900024.
118 M. Song, S. Lee, S. S. T. Nibhanupudi, J. V. Singh, M. Disiena, C. J. Luth, S. Wu, M. J. Coupin, J. H. Warner and S. K. Banerjee, *Nano Lett.*, 2023, **23**, 2952–2957.
119 C. Hu, M. D. McDaniel, A. Posadas, A. A. Demkov, J. G. Ekerdt and E. T. Yu, *Nano Lett.*, 2014, **14**, 4360–4367.
120 X. Zhao, J. Xu, D. Xie, Z. Wang, H. Xu, Y. Lin, J. Hu and Y. Liu, *Adv. Mater.*, 2021, **33**, 2104023.
121 E. R. Kandel, *et al.*, *Principles of Neural Science*, McGraw-Hill Education, New York, NY, 5th edn, 2014.
122 D. Strukov, *et al.*, *Nat. Commun.*, 2019, **10**, 4838.
123 R. Waser, R. Dittmann, G. Staikov and K. Szot, *Adv. Mater.*, 2009, **21**, 2632–2663.
124 T. Ohno, T. Hasegawa, T. Tsuruoka, K. Terabe, J. K. Gimzewski and M. Aono, *Nat. Mater.*, 2011, **10**, 591–595.
125 B. C. Jang, S. Kim, S. Y. Yang, J. Park, J.-H. Cha, J. Oh, J. Choi, S. G. Im, V. P. Dravid and S.-Y. Choi, *Nano Lett.*, 2019, **19**, 839–849.
126 Y.-R. Jeon, D. Akinwande and C. Choi, *Nanoscale Horiz.*, 2024, **9**, 853–862.
127 M. Ismail, H. Abbas, A. Sokolov, C. Mahata, C. Choi and S. Kim, *Ceram. Int.*, 2021, **47**, 30764–30776.
128 Y. Lee, J. Park, D. Chung, K. Lee and S. Kim, *Nanoscale Res. Lett.*, 2022, **17**, 84.
129 J. Suñé, F. Aguirre, M. Bargalló González, F. Campabadal and E. Miranda, *Adv. Quantum Technol.*, 2023, **6**, 2300048.
130 G. Milano, F. Ferrarese Lupi, M. Fretto, C. Ricciardi, N. De Leo and L. Boarino, *Adv. Quantum Technol.*, 2020, **3**, 2000009.
131 Y. Pang, B. Gao, B. Lin, H. Qian and H. Wu, *Adv. Electron. Mater.*, 2019, **5**, 1800872.
132 R. Carboni and D. Ielmini, *Adv. Electron. Mater.*, 2019, **5**, 1900198.
133 M. S. Song, T.-H. Kim, H. Hwang, S. Ahn, H. Nili and H. Kim, *Adv. Intell. Syst.*, 2023, **5**, 2200358.
134 S. Pazos, *et al.*, *Nanoscale*, 2023, **15**, 2171–2180.
135 K. Delfanazari, *et al.*, *Phys. Rev. Appl.*, 2024, **21**, 014051.